Gondwana Research 79 (2020) 49–69

Contents lists available at ScienceDirect

Gondwana Research

journal homepage: www.elsevier.com/locate/gr

The Itmurundy Pacific-type orogenic belt in northern Balkhash, central Kazakhstan: Revisited plus first U–Pb age, geochemical and Nd isotope data from igneous rocks

I. Safonova [a, b, *], I. Savinskiy [a], A. Perfilova [a, b], A. Gurova [a], S. Maruyama [a], T. Tsujimori [c, d]

[a] Novosibirsk State University, Pirogova St. 2, Novosibirsk, 630090, Russia
[b] Sobolev Institute of Geology and Mineralogy, SB RAS, Koptyuga ave. 3, Novosibirsk, 630090, Russia
[c] Center for Northeast Asian Studies, Tohoku University, Aoba, Sendai, 980-8576, Japan
[d] Department of Earth Science, Tohoku University, Aoba, Sendai, 980-8578, Japan

ARTICLE INFO

Article history:
Received 13 June 2019
Received in revised form
7 September 2019
Accepted 10 September 2019
Available online 9 October 2019

Keywords:
Central asian orogenic belt
Paleo-asian ocean
Ordovician-early silurian
Ocean plate stratigraphy
Intra-oceanic arc

ABSTRACT

The Itmurundy zone/belt is located in the northern Balkhash area of central Kazakhstan. Geologically it belongs to the Kazakh orocline located in the western Central Asian Orogenic Belt (CAOB), north of the Tarim craton and west of the Junggar block. The Itmurundy belt, which surprisingly has remained unstudied in terms of up-to-date geochronological, geochemical and isotope methods compared to other regions of the CAOB, was revisited and reinvestigated. The belt possesses a very complicated geological structure and hosts rocks of mantle, orogenic and post-orogenic associations. This paper focuses on the orogenic association and presents original geological data, first U–Pb age and first up-to-date geochemical and Nd isotope data from igneous rocks. The orogenic association of the Itmurundy belt includes volcanic and sedimentary rocks of three formations, Itmurundy ($O_{1\text{-}2}$), Kazyk ($O_{2\text{-}3}$) and Tyuretai (O_3–S_1), and represents an accretionary complex. The most lithologically diverse Itmurundy Fm. ($O_{1\text{-}2}$) consists of oceanic basalt, pelagic chert, hemipelagic siliceous mudstone and siltstone, and greywacke sandstones. Both sedimentary and igneous rocks were strongly deformed by syn- and post-accretion processes, which, in places, formed duplex structures. The igneous rocks are basalt/dolerite/gabbro, andesibasalt, trachybasalt and diorite. The diorite yielded a U–Pb age of ca. 500 Ma. The subalkaline volcanic and subvolcanic rocks belong to the tholeiitic series. Based on major oxides three groups of rocks can be distinguished: high-Ti, mid-Ti and low-Ti. The rocks of these three groups are variably enriched in LREE ($La_N = 122$, 23 and 2 in average, respectively) showing LREE enriched (high-Ti), LREE depleted (mid-Ti) and flat (low-Ti) REE patterns. The high-Ti group shows enrichment in Nb, Th, and Zr compared to the mid-Ti and low-Ti groups. The low-Ti group is special for the Nb troughs in primitive mantle normalized multi-element diagrams, which are typical of supra-subduction settings. The values of εNd are mostly positive for the mid-Ti and low-Ti groups, but negative for the high-Ti group. The geochemical features of the igneous rocks suggest their formation in oceanic (oceanic floor and oceanic island/seamount) and supra-subduction (intra-oceanic arc) settings. In general, the structural position, lithology and deformation styles of Itmurundy sedimentary and igneous rocks and the geochemical features of the igneous rocks all accord well with the models of Ocean Plate Stratigraphy (OPS) and Pacific-type orogeny. Thus, the Itmurundy belt at northern Balkhash represents an Ordovician-Silurian Pacific-type orogenic belt formed at a convergent active margin of the Paleo-Asian Ocean.

1. Introduction

The Itmurundy zone is an important, but greatly understudied constituent of the Central Asian Orogenic Belt (CAOB) or Altaides, the world largest Phanerozoic accretionary orogen (e.g., Zonenshain et al., 1990; Sengör et al., 1993; Mossakovsky et al., 1993; Jahn, 2004; Windley et al., 2007; Kröner et al., 2007, 2014; Safonova, 2017) (Fig. 1). It is located in the western CAOB, at the northern shore of Lake Balkhash (also referred to as Balqash) of central Kazakhstan, south of the Predchingiz Devonian volcanic arc terrane. In the early 1980-ties the Itmurundy belt was called a spillite-jasper complex hosting ophiolites of unclear ages, Neoproterozoic (Riphean to Sinian in old literature), Cambrian or

* Corresponding author. Novosibirsk State University, Sobolev Institute of Geology and Mineralogy SB RASA, Novosibirsk, Russia.
E-mail address: inna03-64@mail.ru (I. Safonova).

https://doi.org/10.1016/j.gr.2019.09.004
1342-937X/

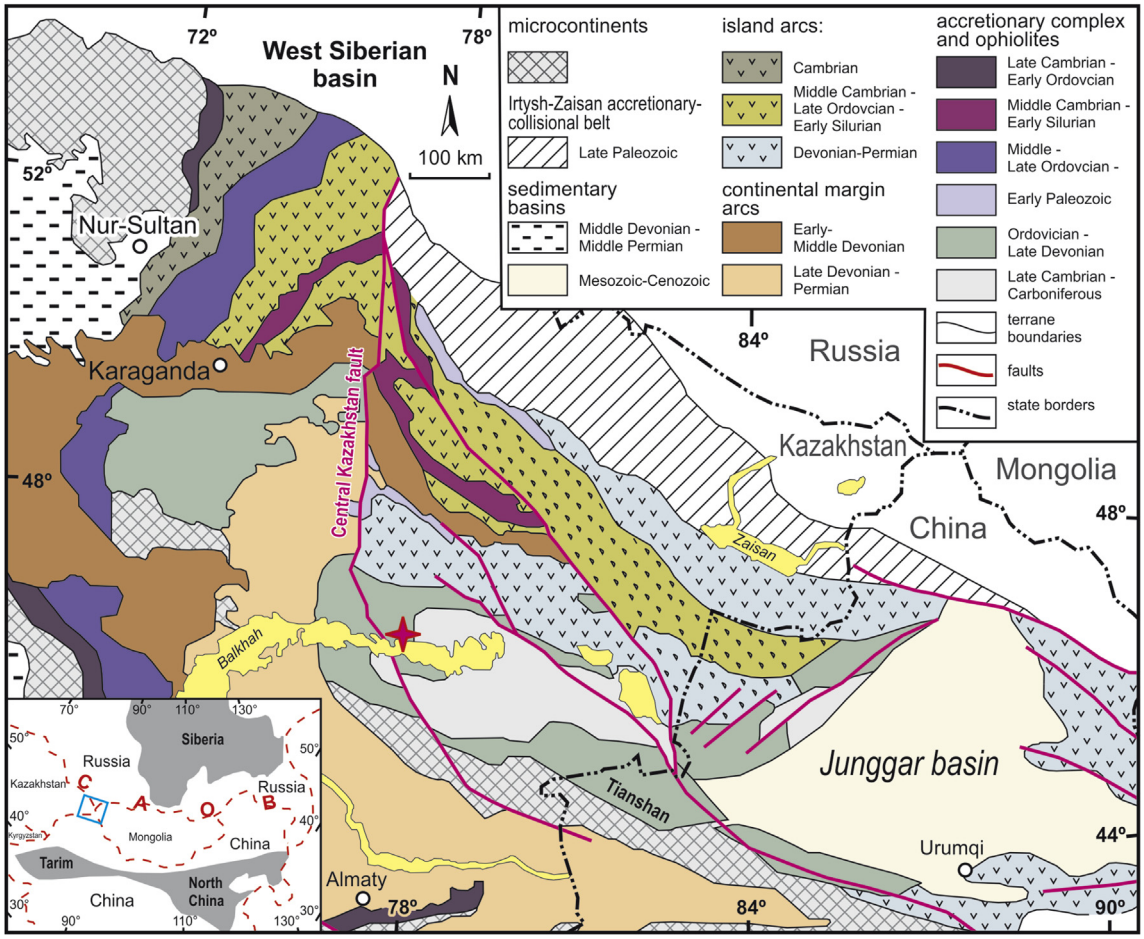

Fig. 1. Simplified tectonic scheme of the western Central Asian Orogenic Belt and location of the Itmurundy belt shown as red star (modified after Windley et al., 2007). (For interpretation of the references to color in this figure legend, the reader is referred to the Web version of this article.)

Ordovician (Patalakha and Belyi, 1981). Since the late 1990-ies and 2000-s this belt has been classified as an accretionary prism or complex (Zhylkaidarov, 1998; Stepanets, 2016), which formation was related to the evolution of the Paleo-Asian Ocean (PAO) and its further suturing and formation of the CAOB (Dobretsov et al., 1995, 2003; Buslov et al., 2001; Safonova and Santosh, 2014). The Itmurundy belt occurs as a complex of intricately folded thrust sheets and tectonic blocks partly transformed into a polymictic and/or serpentinitic melange (Ermolov et al., 1990) composed of rock units of different tectonic origins (Fig. 2). It is dominated by several kilometers long and wide bodies of ultramafic rocks, gabbro, basalt and andesibasalt, chert, siliceous mudstone, siltstone and shale, and sandstones (Fig. 2). The Itmurundy belt is known for hosting a large deposit of jadeite (Patalakha and Belyi, 1981; Kovalenko et al., 1994).

Earlier studies considered the Itmurundy oceanic units (basalts and sediments) as formed in a back-arc basin/marginal sea (Ermolov et al., 1990; Stepanets, 2016). However, the abundant igneous and sedimentary rocks of obviously oceanic origin and the very limited micropaleontological data from Ordovician siliceous sediments, chert and mudstone (Novikova et al., 1983; Nikitin et al., 1991, 1992; Zhylkaidarov, 1998; Nikitin, 2002), suggest a time interval and environments of sedimentation corresponding to a larger and deeper oceanic realm. In addition, the limited geochemical data from mafic volcanic rocks (Stepanets, 2016) and their association with oceanic sediments (ribbon chert) (Patalakha and Belyi, 1981) suggest that the volcanic rocks erupted in an oceanic setting. Finally, after a more than 30 years gap, the geological features of the Itmurundy belt and the problems related to its study were re-evaluated and re-focused in a recent paper by (Safonova et al., 2019).

Several localities of intra-oceanic arcs and oceanic crust of Ordovician age sensu stricto have been reported in the western CAOB: in Altai, Kazakhstan and western Junggar (Safonova et al., 2017 and references therein). The Russian Altai hosts fragments of oceanic crust of late-Cambrian to early Ordovician age (e.g., Iwata et al., 1997; Sennikov et al., 2003; Safonova et al., 2011). The Ordovician Selety-Urumbai, Bozshakol-Chingiz, Baydaulet-Aqbastau intra-oceanic arc terranes occur in northern and eastern Kazakhstan (Shen et al., 2007; Degtyarev, 2011, 2012). Several localities of Ordovician ophiolites have been reported in western Junggar (e.g., Wang et al., 2003; Liu et al., 2016; Zhang et al., 2018). The origin of the Itmurundy ophiolites, in particular, their age and petrogenesis, have remained enigmatic as no detailed geochronological or geochemical studies have been ever accomplished in northern Balkhash region. According to our own geological data (Safonova et al., 2019) and previous publications (Zhylkaidarov, 1998; Stepanets, 2016), in this paper we refer the Itmurundy zone to as “Itmurundy belt” including an accretionary complex and an ophiolite belt. We review and integrate the available data from the Itmurundy belt, though limited, and revisit this geological entity in terms of its geological structure, rock assemblages, age, deformation features and modern concepts on the origin of ophiolites and accretionary complexes. We present first U–Pb zircon ages and up-to-date geochemical and isotope data from Itmurundy igneous rocks. We will show that the Itmurundy belt

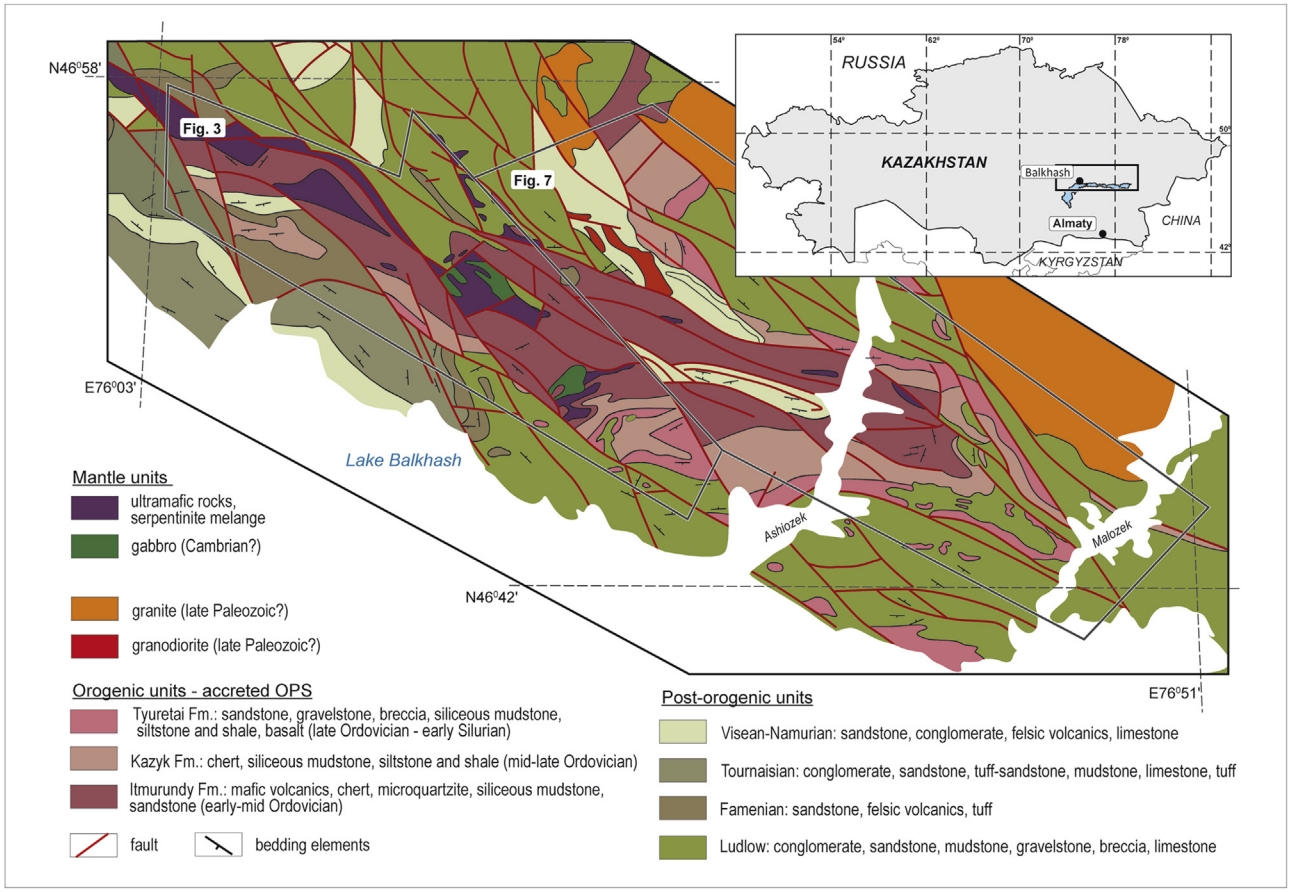

Fig. 2. Geological map of the Itmurundy belt in northern Balkhash, central Kazakhstan, and index map of the Itmurundy region in Kazakhstan – modified from the 1/200,000 scale Geological map of the USSR, Sheet L-43-XI (Koshkin and Galitsky, 1960).

records a story of a much wider/deeper ocean, than considered before (Stepanets, 2016), and give first constrains on the lifetime of the ocean based on the field observations and careful mapping of outcrops. Finally, we will propose reconstructions of the accretionary complex in terms of the model of Ocean Plate Stratigraphy (OPS; e.g., Isozaki et al., 1990; Maruyama et al., 2010; Kusky et al., 2013) and its tectonic history in the context of the whole history of the western CAOB. In this paper we present first up-to-date analytical data, U–Pb zircon ages, major and trace elements, and whole-rock Nd isotopes, from igneous rocks: gabbro, basalt, andesibasalt, and dolerite (analytical details are provided in Supplementary Electronic Materials). The rocks were sampled at Horse-1 and Horse-2 sites in the central part of the Itmurundy AC (Figs. 2, 3 and 6, 1S).

2. Geology of the Itmurundy region

The Itmurundy or Itmurundy-Kazyk zone, including ophiolite belt and/or accretionary complex, is a part of the Junggar-Balkhash foldbelt, which extends to the western Junggar region in NW China (Fig. 1) (e.g., Patalakha and Belyi, 1981; Ermolov et al., 1990; Kurenkov et al., 2002; Windley et al., 2007). In the 1/200,000 geological map (Koshkin and Galitsky, 1960) we can recognize three main units or assemblages of rocks: mantle, orogenic and post-orogenic, which are separated from each other by regional to local faults (Figs. 2 and 3; Table 1). The mantle assemblage consists of probably pre-Ordovician peridotites, dominantly dunite and wherlite, plus gabbro, i.e. it represents lower parts of an ophiolitic package. The orogenic assemblage includes mafic volcanic rocks (mostly basalt, dolerite), ribbon chert, hemipelagic siliceous thin-grained sediments (mudstone, siltstone, shale), gray and greenish-gray sandstones and flyschoid greywacke sandstones. The Ordovician to early Silurian ages of the siliceous sediments were constrained by microfossil data (Novikova et al., 1983; Nikitin et al., 1991, 1992; Zhylkaidarov, 1998; Nikitin, 2002; Safonova et al., 2019). We use term "orogenic" because these rocks obviously formed in oceanic environments and were piled up together during Pacific-type orogeny and related accretion. They remained on the surface only due to the orogeny, otherwise they would subduct to the deep mantle (Maruyama et al., 2011; Safonova, 2017). Second, a part of sedimentary rocks is directly related to orogeny (arc-derived sandstones, trench facies, etc.), therefore they "have a right" to be considered as part of orogenic units. Third, we cannot separate those sedimentary rocks in accretionary complexes– they occur together, often intercalated, therefore, they all, both terrigenous/clastic and oceanic, both volcanic (basalts having mantle origin) and sedimentary, belong to a single unit formed as a result of Pacific-type orogeny.

The "post-orogenic" assemblage including the rocks formed after the Pacific-type orogeny at the active margins of the PAO and its suturing, consists of mid-Silurian to Carboniferous continental margin to continental sediments (sandstones, carbonates, conglomerates) and felsic volcanic rocks. Hereinafter we will refer the mantle assemblage to as Itmurundy ophiolite complex and the orogenic assemblage to as Itmurundy accretionary complex (Fig. 2).

The Itmurundy ophiolite belt consists of folded thrust sheets, which are, in places, deformed and broken to form polymictic mélange (Ermolov et al., 1990). It includes three ultramafic-mafic massifs: Kentaralau in the west (dominated by harzburgite and serpentinite), Itmurundy in the centre (dominated by dunite), and Arkharsu in the east (dominated by serpentinite mélange, wehrlite,

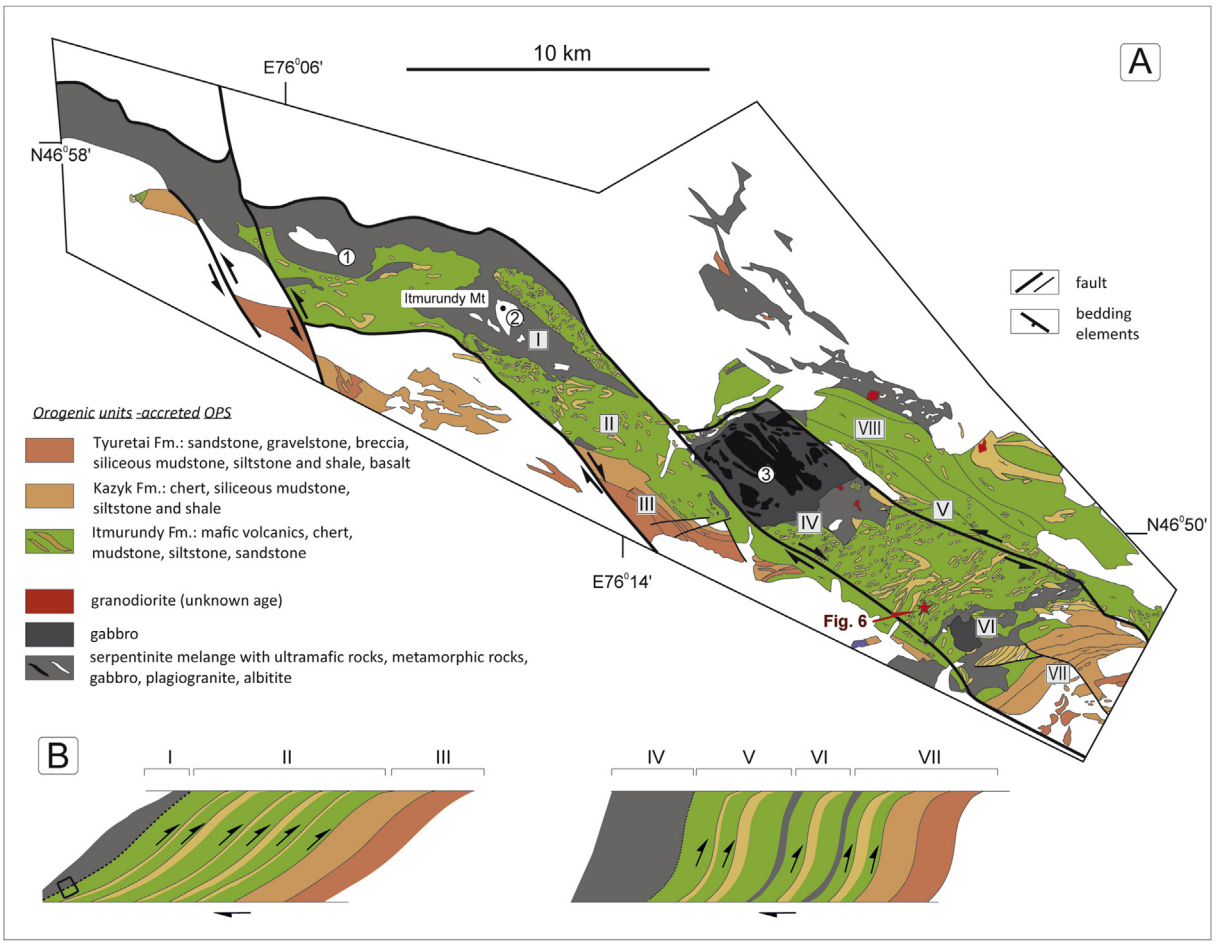

Fig. 3. A, Geological map of the Itmurundy accretionary complex, central Kazakhstan (modified from Patalakha and Belyi, 1981). B, duplex structures consisting of OPS packages (horses) of the Itmurundy, Kazyk and Tyuretai formations. Numbers in circles are for the Kentaralau (1), Itmurundy (2) and Arkharsu (3) ultramafic-mafic massifs.

Table 1
Description of the igneous rocks sampled in the Itmurundy accretionary complex.

	sample no.	Rock type	Mode of occurrence	site name[a]	Coordinates
1	IT-05-17	dolerite	small outcrop	H2	N 46°48′36.7″; E 76°20′40.2″
2	IT-13-17	aphyric basalt	lava flow	H2	N 46°48′49.8″; E 76°20′45.1″
3	IT-16-17	microgabbro	core of lava flow	H2	N 46°49′04.6″; E 76°20′53.2″
4	IT-22-17	aphyric basalt	lava flow	H2	N 46°48′59.0″; E 76°20′49.8″
5	IT-35-17	dolerite	lava flow	OD1	N 46°43′09.05″; E 76°44′47.1″
6	IT-36-17	porphyric basalt	pillow-lava	OD1	N 46°43′06.3″; E 76°44′34.4″
7	IT-43-17	amygdaloidal basalt	pillow-lava	H2	N 46°49′39.6″; E 76°21′23.3″
8	IT-44-17	basalt	pillow-lava	H2	N 46°49′36.9″; E 76°21′24.4″
9	IT-60-17	aphyric basalt	pillow-lava	H2	N 46°48′19.1″; E 76°21′38.5″
10	IT-61-17	porphyric basalt	pillow-lava	H2	N 46°48′17.7″; E 76°21′32.3″
11	IT-62-17	porphyric basalt	pillow-lava	H2	N 46°48′18.3″; E 76°21′38.2″
12	IT-63-17	aphyric basalt	pillow-lava	H2	N 46°48′14.5″; E 76°21′39.3″
13	IT-64-17	aphyric basalt	pillow-lava	H2	N 46°48′13.2″; E 76°21′40.2″
14	IT-73-17	microgabbro	small outcrop	H2	N 46°49′53.1″; E 76°18′29.0″
15	IT-75-17	microgabbro	small outcrop	NW H2	N 46°52′47.5″; E 76°16′40.2″
16	IT-76-17	porphyric basalt	pillow lava	NW H2	N 46°52′41.4″; E 76°16′55.2″
17	IT-77-17	aphyric basalt	lava flow	NW H2	N 46°52′46.8″; E 76°17′08.7″
18	IT-78-17	aphyric basalt	lava flow	NW H2	N 46°52′48.6″; E 76°17′21.4″
19	IT-79-17	aphyric basalt	lava flow	NW H2	N 46°52′21.4″; E 76°17′08.7″
20	IT-80-17	gabbro-dolerite	small outcrop	NW H2	N 46°52′50.0″; E 76°17′37.6″
21	ИХ-14	microgabbro	core of lava flow	H2	N 46°48′19.2″; E 76°22′21.2″
22	H2-14	gabbro	outcrop	H2	N 46°50′59.9″; E 76°17′39.5″
23	H2-15-1	microgabbro	outcrop	H2	N 46°50′59.5″; E 76°17′53.9″
24	H2-16-1	clastic lava	outcrop	H2	N 46°50′56.0″; E 76°18′09.8″
25	N17008	aphyric basalt	lava flow	H2	N 46°48′31.8″; E 76°21′25.8″
26	17081902	aphyric basalt	lava flow	H2	N 46°49′50.8″; E 76°18′27.8″
27	JD6-1	diorite	small outcrop	western	N 46°57′02.2″; E 76°03′04.5″

Sites: H1 – Horse-1, H2 – Horse-2, NW - northwestern.
[a] See Figs. 1 and 2 for details.

pyroxenite and gabbro) (Fig. 3). There are plagiogranite and sodium-metasomatic rocks formed after the ultramafic rocks at the periphery of the ophiolite complex, whereas jadeite and jadeitite-albitite occur in the central part (Patalakha and Belyi, 1981; Kovalenko et al., 1994).

A zone of polymictic mélange is located in the northern part of the Itmurundy belt (Figs. 2 and 3). The polymictic mélange consists of sheared dunite-harzburgite serpentinite hosting blocks of lherzolite, pyroxenite, jadeite, gabbro, gabbro-amphibolite, dolerite, altered basalt (greenstone), albitite, plagiosyenite, plagiogranite, amphibolite, garnet-epidote-muscovite, actinolite and glaucophane schists, apoeclogite garnet amphibolite (Antonyuk, 1974; Avdeev, 1986). Wherlite and lherzolite often form ultramafic bodies. The ultramafic rocks are typically strongly serpentinized. The serpentinitic rocks are dominated by chrysotile-lizardite-harzburgite serpentinite with relicts of olivine and orthopyroxene and lizardite-antigorite and antophyllite-antigorite serpentinites, with subordinate dunitic serpentinites. The harzburgite serpentinite is often cut by veins of pyroxenite. The high-pressure rocks from the outcrops of the mélange located north of Mountain Itmurundy yielded ages from 468 to 458 Ma, unfortunately, no analytical details were provided in (Ermolov, 2008). Of special interest are apoeclogitic garnet amphibolite and glaucophane schists (Ermolov P.V., pers. comm.). The garnet amphibolite contains omphacite, garnet and rutile and the glaucophane schist formed after basalt (Ermolov et al., 1990). The rocks are submerged into serpentinite matrix showing, in places, boudinage and schistosity. The granitic rocks are plagiogranites spatially associated with ultramafic rocks (Patalakha and Belyi, 1981).

Outcrops of another type of serpentinite mélange, monomictic, occur in the central and southern parts of the belt (Fig. 3A). The mélange consists of serpentinite with relatively well preserved blocks of ultramafic rocks (Kovalenko et al., 1994). The northern polymictic serpentinite mélange is separated from the central monomictic serpentinite mélange by an accretionary complex consisting of tectonic sheets of basalts associated with chert, siliceous shale, siltstone and mudstone, and sandstone.

Accretionary complexes typically consist of igneous and sedimentary rocks scrapped off the subducting oceanic plate: basalt, chert, mudstone, siltstone and shale, sandstone. Those units compose what we know as Ocean Plate Stratigraphy or OPS (e.g., Isozaki et al., 1990; Maruyama et al., 2010; Kusky et al., 2013; Safonova and Santosh, 2014; Safonova et al., 2016). The Itmurundy accretionary complex also includes volcanic and subvolcanic rocks of basaltic and andesibasaltic composition, pelagic sediments (ribbon chert), hemipelagic sediments (siliceous mudstone, siltstone and shale) and trench sediments (turbidite, sandstone, conglomerate) (Figs. 3 and 4, 5A-C).

The accreted tectonic sheets are overlain by a neoautochtonous olistostrome emplaced over a Famenian basal horizon consisting of conglomerate with pebbles of chert (Ermolov et al., 1990). The olistostrome is then overlain by gravelstone and greenish-gray and lily sandstone and mudstone. Up the section there is another unconformity, a thrust, separating the lower units from probably early Carboniferous gray and motley polymictic sediments: conglomerates, gravelstone, sandstone and mudstone. Unlike the Famenian olistostrome, the upper basal horizon contains pebbles of basalt, granitoids and chert as well as olistoliths of basalt and ribbon chert (Ermolov et al., 1990). The northern margin of the Itmurundy belt is unconformably overlain by late to early Carboniferous sedimentary units (Fig. 2).

3. Stratigraphy of the Itmurundy belt

The stratigraphy of the Devonian volcanogenic-cherty formations of the south-western Predchingiz terrane, which is located north to the Itmurundy zone (Fig. 1) is generally well understood (Degtyarev, 2011), but the lithologically similar strata of the northern Balkhash Region, first of all, the Itmurundy belt, are still a subject of debates in respect to both, their age and tectonic affinity. The Itmurundy belt has a very complicated structure (Fig. 3A), which makes its stratigraphic subdivision problematic. According to the geological map (Koshkin and Galitsky, 1960, Fig. 2) the rocks of the accretionary complex belong to three main formations (bottom to top): Itmurundy, Kazyk and Tyuretai (Figs. 2 and 4; Table 1). Due to the deficiency of well-preserved fossils and strong deformations those formations are shown as late Neoproterozoic to Cambrian in the 1950–1960 geological maps (e.g., Koshkin and Galitsky, 1960). Later findings of microfauna (conodonts, graptolites) showed their younger age, Ordovician to early Silurian (Novikova et al., 1983; Nikitin et al., 1991, 1992; Ermolov et al., 1990; Zhylkaidarov, 1998; Nikitin, 2002).

The Itmurundy Fm. consists of basalt (at the base of most sections), gray and brown ribbon cherts, chocolate, red, brown and greenish gray siliceous mudstones, siltstones and shales plus rare outcrops of sandstone (Figs. 4, 5A-C; Safonova et al., 2019). The lower part of the Itmurundy Fm. is dominated by basalt and overlying chert, while the middle part consists of basalt, chert and siliceous mudstone. The upper part of the formation contains coarser grained sediments, such as siliceous mudstone, siltstone and sandstone plus gravelstone and breccia plus subordinate basalt and chert. The first evidence for the Ordovician (not late Neoproterozoic) age of the Itmurundy Fm. came from the chert hosted Ordovician conodonts found by Novikova et al. (1983). Later, early Ordovician (Tremadocian to Floian) conodonts *Paroistodus proteus Lindstrom* and late Ordovician (lower Sandbian) conodonts *Periodon aculeatus Hadding, Pygodus* cf. *serra (Hadding), Pygodus* cf. *anserinus Lamont & Lindström* were recovered from chert and semi-transparent silicilite exposed at the base and top of the Karazhal ridge, respectively (Ermolov et al., 1990). The silicilite probably represents recrystallized chert or siliceous mudstone. Thus, we accept the age of the Itmurundy Fm. as lower-middle Ordovician.

The rocks of the Itmurundy Fm. are separated from those of the Kazyk Fm. by faults (Figs. 2 and 3A). The Kazyk Fm. is dominated by red and brown ribbon chert, siliceous mudstone, siltstone and shale with subordinate basalt (Figs. 4 and 5B). Chert yielded Ordovician conodonts: Pygodus serra (Hadding, 1913) and P. cf. anserinus Lamont & Lindstrom, 1957 (Novikova et al., 1983) and Pygodus serra and P. anserinus - late Llanvirn (Kurkovskaya, 1985; Zhylkaidarov, 1998). Thus, the previous data on conodonts suggest that the Itmurundy and Kazyk Fms. are of close ages - middle–upper Ordovician - roughly corresponding to the Llandeilian Pygodus anserinus Zone. Our original age data from conodonts extracted from a chert of the Kazyk Fm. show the age range from the late Middle Ordovician ($O_{2\text{-}3}$) to the early Late Ordovician ($O_{1\text{-}3}$) (Safonova et al., 2019). Thus, we accept the age of the Kazyk Fm. as middle-upper Ordovician.

The rocks of the Tyuretai Fm. are also separated from those of the Kazyk Fm. by faults (Figs. 2 and 3A). The formation is dominated by coarser grained clastic sediments - siliceous mudstone, siliceous siltstone and sandstone with subordinate basalt and chert (Fig. 4). The Tyuretai cherts contain upper Ordovician conodonts within the Pygodus anserinus Zone (Zhylkaidarov, 1998; Novikova et al., 1983; Kurkovskaya, 1985). The Tyuretai siliceous siltstones yielded early Silurian graptolites Demirastrites triangulatus, Glyptograptus tamariscus vasians, G. nicolaevi, and other species typical of the Llandovery (Koshkin et al., 1987).

The main lithologies of these three formations match the OPS model or succession (basalt – chert – siliceous mudstone/siltstone - sandstone) (Isozaki et al., 1990; Maruyama et al., 2010; Safonova et al., 2016, 2019). Thus, the Itmurundy Fm. is dominated by basalt and chert (lower OPS - pelagic), the Kazyk Fm. - by chert and

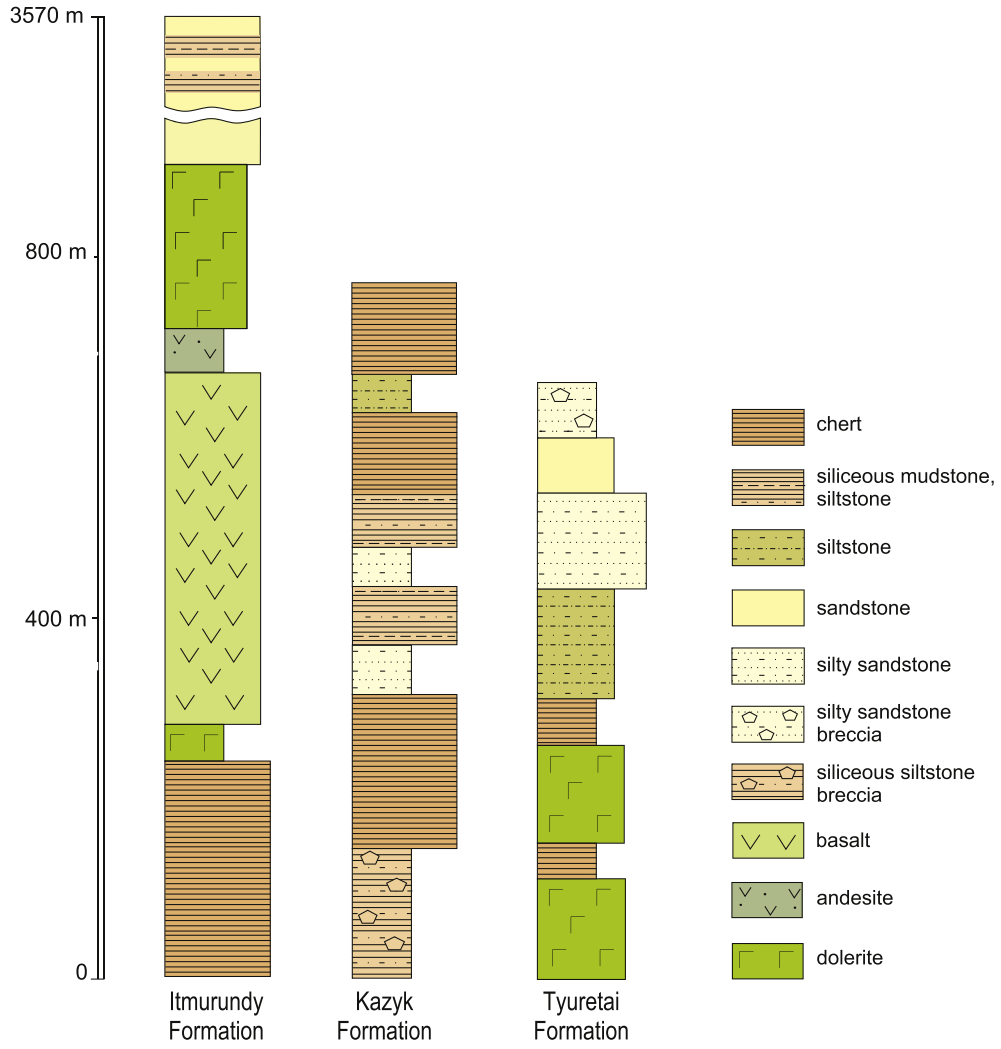

Fig. 4. Lithological columns of the Itmurundy (early-middle Ordovician), Kazyk (middle-late Ordovician) and Tyuretai (late Ordovician-early Silurian) formations of the Itmurundy accretionary complex, central Kazakhstan (modified from Patalakha and Belyi, 1981).

siliceous mudstone, siltstone and shale (middle OPS – pelagic plus hemipelagic), and the Tyuretai Fm. - by siliceous hemipelagic sediments and trench sandstones (upper OPS - turbidites, conglomerates).

4. Structure and deformation patterns

The tectonic framework of the Itmurundy belt includes three groups of faults striking ca. from (1) WWN to EES (az. 300–310°), (2) north to south (az. 350-10°) and (3) from NE to SW (az. 60–70°) (Figs. 2 and 3A). The first group includes large regional faults separating the post-orogenic association from the mantle and orogenic associations (Fig. 2). The second group includes medium-scale faults separating the mantle and orogenic associations (Fig. 3A). The third group includes small faults separating packages consisting of OPS sediments of the orogenic association (Fig. 6). These fault systems form the blocky structure of the Itmurundy belt (Figs. 2 and 3A). Fault groups 2 and 3 reflect accretion related thrusting. They form duplex units separated by top and bottom thrusts duplicated through time (Fig. 3B). Each of them is sub-divided into several horses by linking thrusts. The horses consist of OPS rocks (basalt, chert, siliceous mudstone/siltstone), which stratigraphy face top to the south or south-east (Fig. 3B). The faults of Group 1 probably developed in a regime of compression: the geological map show they were active during the formation (extrusion/exhumation?) of ultramafic bodies and were coeval with shearing and boudinage. They can be classified as post-orogenic faults, which are dominated by high-angle strike-slip faults and defined by cutting relationships possibly related to the collisional episodes following oceanic suturing and subsequent orogeny. Accordingly, the accretionary complex can be divided into eight segments (I to VIII) separated by Group 3 faults. Each segment is cut by linking thrusts to form several horse structures (Figs. 3 and 6).

The three groups of faults separate three blocks, western, central and eastern, all consisting of OPS units (Fig. 3A). The western block (segments I to III) includes a major part of the mantle association, e.g., the Itmurundy and Kentaralau ultramafic massifs, Itmurundy Fm. mafic volcanic and subvolcanic rocks with subordinate oceanic sediments, Kazyk Fm. chert and siliceous mudstone, and Tyuretai Fm. hemipelagic rocks and sandstone. The chert units occur over the volcanic rocks.

The central segment (V) represents a horse-structure (Figs. 3A and 6) and includes Itmurundy Fm. rocks. The horse is bounded by faults from north and south which can be interpreted as top and bottom thrusts. The thrusts and thrusting related deformations can be easily identified by strongly sheared basalt, chert and siliceous mudstone as well as by the presence of large chert boudins within basalts and, vice versa, by the fragments of basalt submerged into

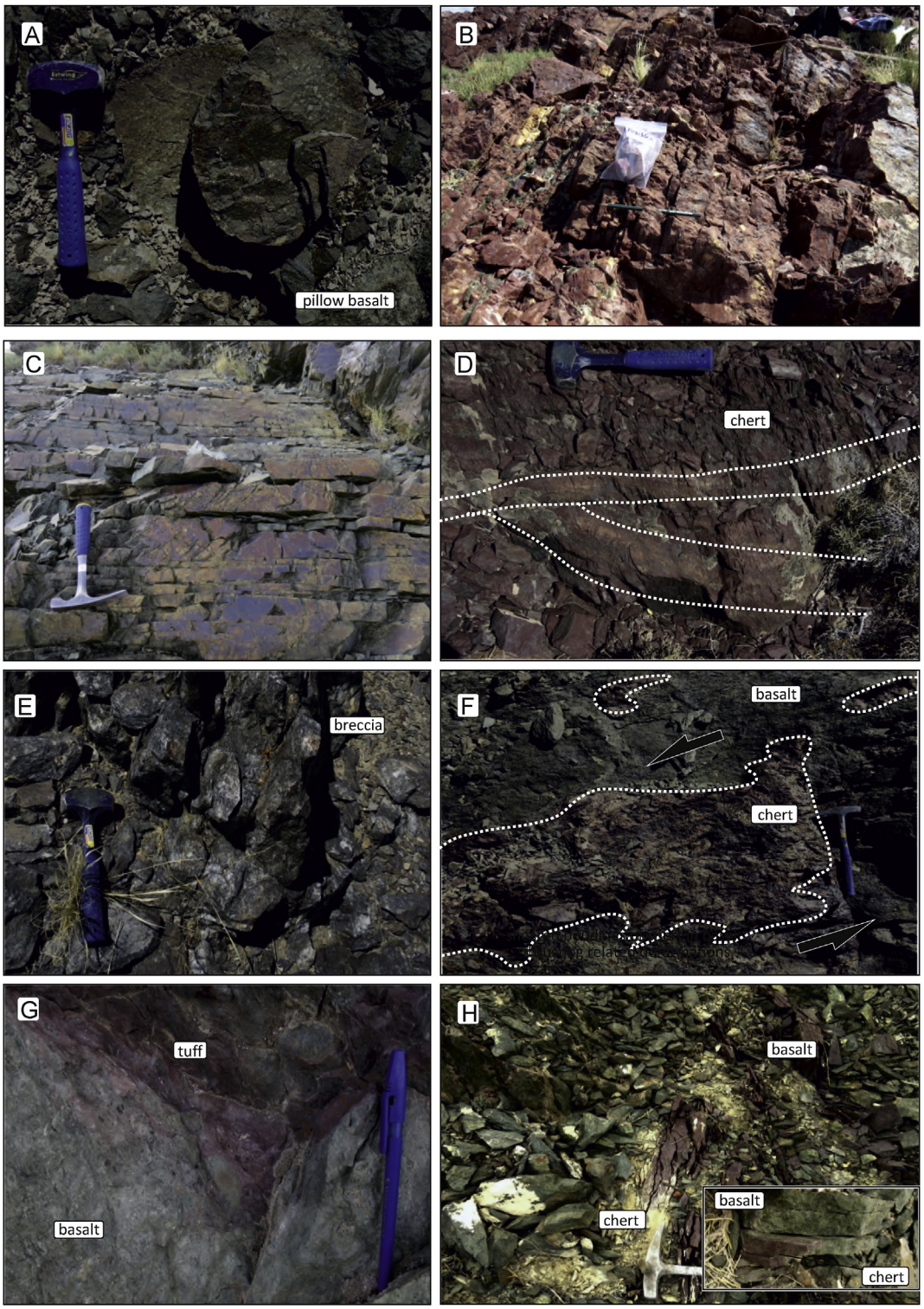

Fig. 5. Photos of outcrops and rocks of the Itmurundy accretionary complex, central Kazakhstan. A, pillowed basalt; B, pelagic ribbon chert; C, siliceous mudstone; D, duplex structures in chert; E, volcanic breccia; F, sheared boudines of chert in basalt; G, sheared basalt and tuff; H, direct cold contact between aphyric basalt and siliceous mudstone.

cherty matrix (Fig. 5F). The central part of the horse is dominated by volcanic rocks: pillowed-basalt with pillows ranging from 15 cm to 1 m in diameter (Fig. 5A) and flows of aphyric and porphyric mafic to andesitic volcanics. During the 2017 field mission we documented a direct cold contact between aphyric basalt and siliceous mudstone (Fig. 5H). Chert (Fig. 5B) and siliceous mudstone (Fig. 5C) crop out at the summits of small hills. The chert and siliceous mudstone often occur in direct contact with underlying basalt showing the signs of duplexing (Fig. 5D) by thrusting and folding (closer to the top) and shearing (closer to the bottom) (Fig. 5H). The cherts are red, greenish, white and black. The ribbons are 2–20 cm thick and are intercalated with clay/mudstone. The sedimentary rocks of the horse carry signatures of thrusting: the lenses of red siliceous mudstones are displaced along the variably

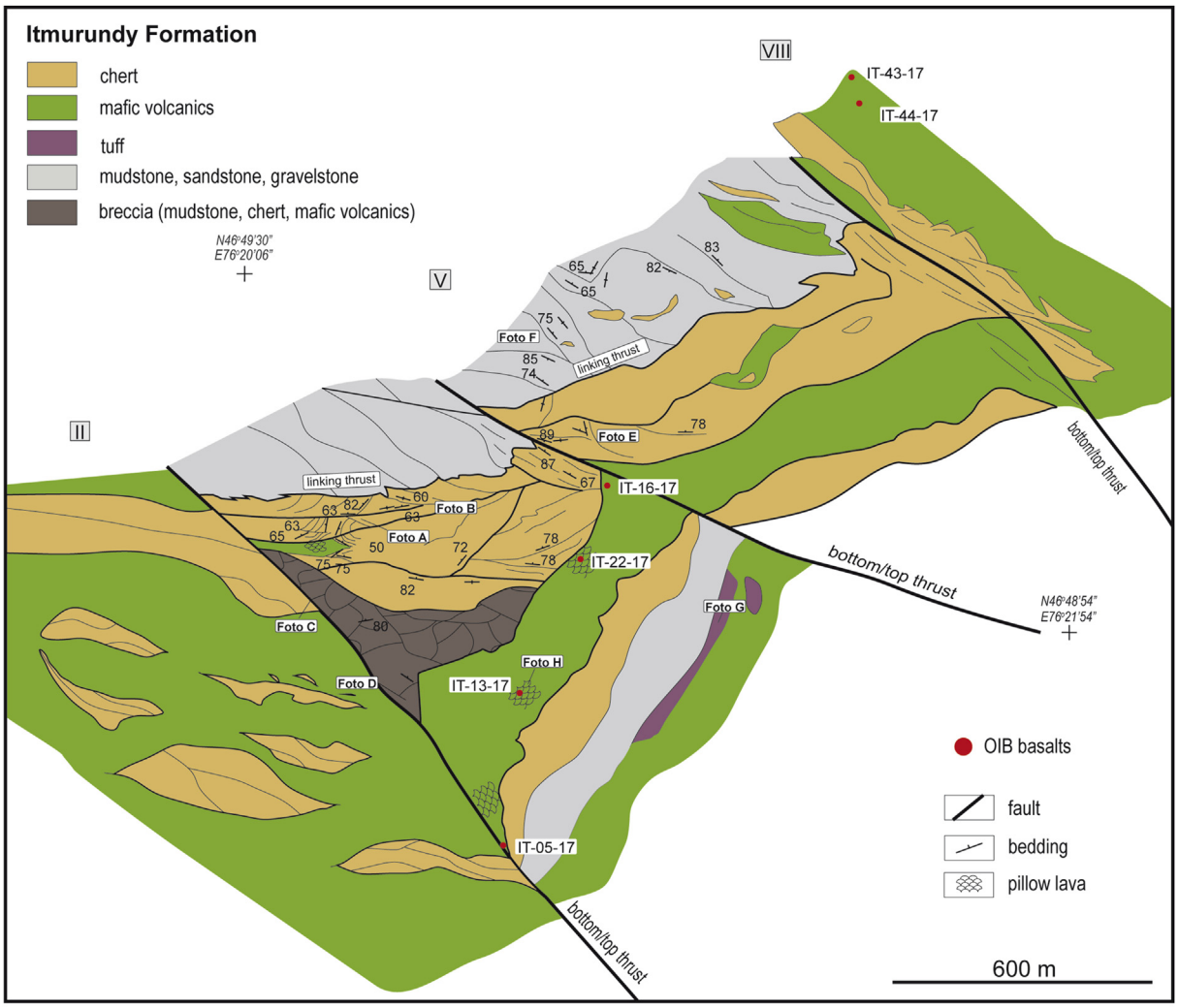

Fig. 6. Geological scheme of a duplex structure in the central Itmurundy accretionary complex, central Kazakhstan – location see in Fig. 3.

colored cherts and along the unconformities inside the cherts (Fig. 5B). In the northern part there are steeply dipping sheared breccia (Fig. 5E), tuff (Fig. 5G) and sandstone. The combination of duplexes (Fig. 5D), mullion structures, isoclinal and asymmetrical folds, vertically dipping sedimentary beds and NW striking beds suggest a compressive regime induced by accretionary tectonics.

The easternmost segment of the Itmurundy belt is a so-called overturned duplex (OD) named after a similar structure featured in the Inuyama area of the Mino accretionary complex, Japan – the OPS world type locality (Matsuda and Isozaki, 1991; Hori, 1992; Safonova et al., 2016) (Fig. 7). Structurally, the OD represents a relatively large isoclinal fold, which NE striking axial plane is parallel to the major faults. The core of the fold consists of Itmurundy Fm. basalts, whereas the flanks are siliceous mudstones and siltstones and gray sandstones of the Kazyk and Tuyretai Fms. The fold is locally broken by normal and reverse faults. Similarly to the central segment those features of folding and faulting could be formed by collisional processes during oceanic closure.

5. Main types and petrography of igneous rocks

The older maps and papers show a layered ultramafic complex in the western part of the Itmurundy belt consisting of wherlite and lherzolite (Fig. 8A). The ultramafic rocks are typically strongly serpentinized. The serpentinized varieties are dominated by loopy chrysotile-lizardite harzburgite serpentinite with relicts of olivine and orthopyroxene, and lizardite, antigorite and antophyllite-antigorite serpentinites plus subordinate dunitic serpentinites. In places, the harzburgite serpentinite is cut by pyroxenite veins. Of special interest are apoeclogitic garnet amphibolite and glaucophane schists. Petr Ermolov and co-authors mention garnet amphibolites with omphacite, garnet and rutile and glaucophane schists formed after basalt although no information about precise location of those rocks have been reported so far (Ermolov et al., 1990).

Another typical rock type is mélange (see section 2) consisting of basalt and basaltic andesite (70%), chert (25%) and trachyandesite, trachyte, alkalite rhyolite and plagiogranite (5%) (Stepanets, 2016). Basaltic rocks occur as pillow lavas of porphyric and aphyric subalkaline basalt, andesibasalt, and alkaline basalt. The porphyric inclusions are plagioclase and diopside. The basalts from the "deep-marine" olistostrome exposed near Karazhal Mt. also represent pillow lavas. Unlike the Itmurundy mélange basalt, the Karazhal porphyric and aphyric basalts are, in average, more vitreous, and have igneous contacts with chert (Ermolov et al., 1990).

Fig. 8 shows major petrographic varieties from the samples collected during the 2017 and 2018 field missions of our team: basalt, andesibasalt, gabbro, dolerite and diorite (Figs. 3 and 6). Basalt and andesibasalt possess aphyric and porphyric (up to aphanitic) microstructures and massive and amygdaloidal textures

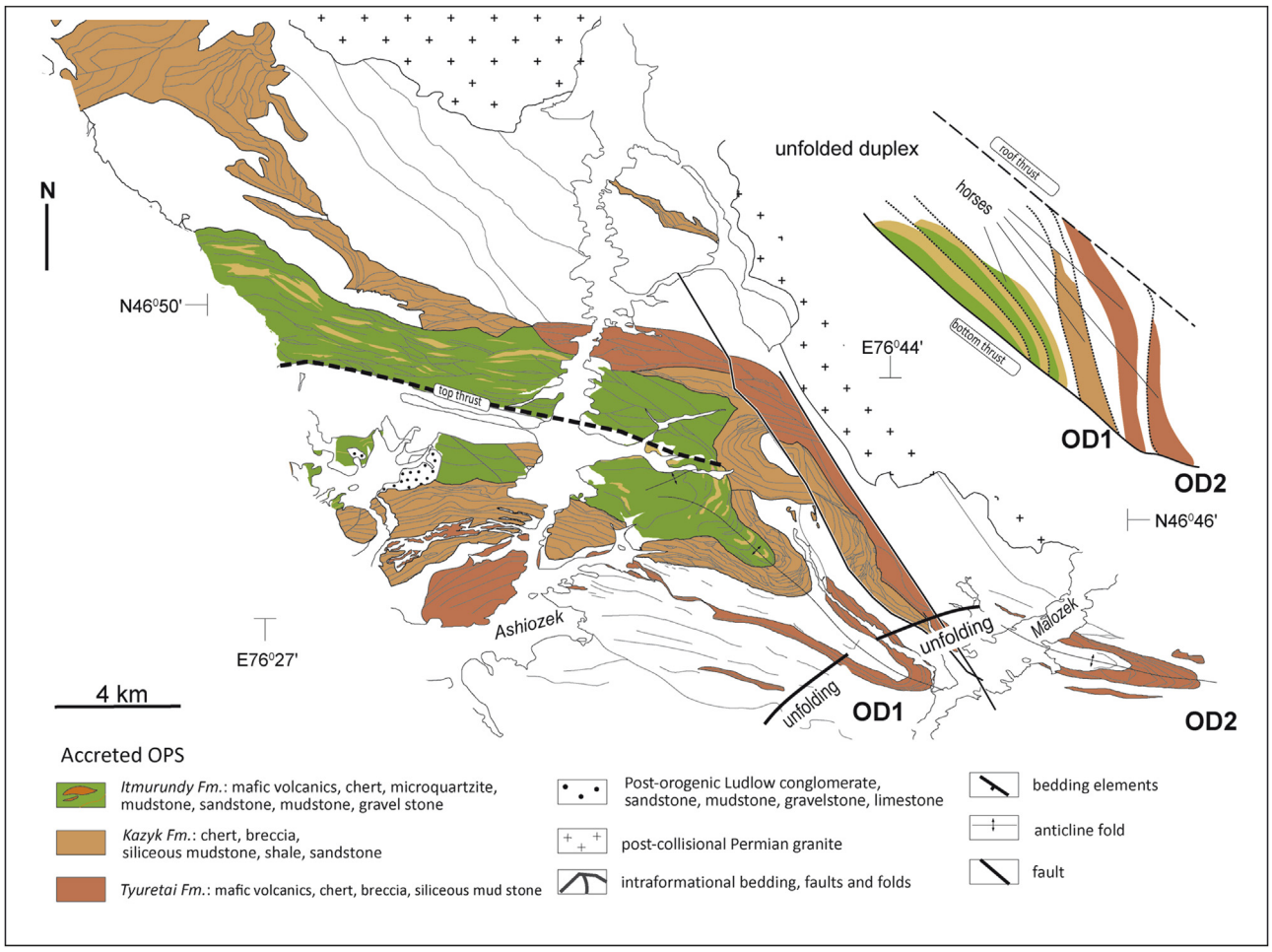

Fig. 7. Geological scheme of the eastern Itmurundy accretionary complex, central Kazakhstan (location see in Fig. 2) with overturned/folded duplex structures OD1 and OD2. An interpretation of unfolded OD1 is shown in the right upper corner.

(Fig. 8C, E). The dolerites and gabbro-dolerite have intercertal, doleritic, microlithic, and poikilophitic microstructures and massive textures. The porphyric varieties typically consist of fine-grained matrix with small to medium-sized (0.1–3 mm) phenocrysts of olivine, clinopyroxene and plagioclase or their glomeroporphyric intergrowths (Fig. 8B, G). The volume percentage of phenocrysts is variable: from 5% to 20%. Olivine phenocrysts (0.1–1 mm) are commonly subhedral (Fig. 8D) and free of compositional zoning. Clinopyroxene phenocrysts are euhedral to subhedral (0.5–1 mm) (Fig. 8B, H). Plagioclase commonly occurs as a phenocryst phase (1–3 mm), some samples containing also plagioclase laths (microlites) in their microcrystalline groundmass (Fig. 8G) and in aphyric varieties (Fig. 8C). Plagioclase phenocrysts and microlites are often albitized/saussuritized. Opaque minerals form euhedral and subhedral microcrysts that range from 0.1 to 0.4 mm (Fig. 8B). The groundmass of porphyric varieties consists of volcanic glass, plagioclase, pyroxene and actinolite microliths and opaque minerals. Upon macroscopic and microscopic investigations, the samples show medium to strong alteration of olivine and pyroxene phenocrysts along rims and cracks and of the groundmass resulting in significant chloritization and epidotization. Secondary prehnite is also common. The microlithic minerals and volcanic glass are altered to epidote, zoisite, chrolite, leucoxene and carbonate. The amygdules are filled by calcite and chlorite (Fig. 8E). The fully crystallized varieties possess doleritic or gabbroic microstructures (Fig. 8H and I). The opaque minerals are often replaced by iron hydroxides.

6. Results

6.1. First U–Pb zircon ages

Several zircon grains were separated from hornblende diorite sampled in the western part of the Itmurundy belt, at the Itmurundy serpentinite melange (Figs. 2, 3 and 8I). The zircons have variable shape and size. There are relatively isometric grains from 20 to 50 μm in diameter and elongated grains up to 400 μm long. The color ranges from colorless to light yellow or brownish. Most grains are transparent or translucent, but all are strongly fractured which made the dating challengeable. Consequently only two grains yielded concordant (99%) ages of 522 ± 7 and 487 ± 5 Ma as seen in the concordia plot (Fig. 9). Two more grains showed ages of 536 ± 5 and 499 ± 4 Ma at lower concordances of 89 and 90%, respectively. Accordingly, we consider the late Cambrian-early Ordovician age as the most probable age of the formation of the Itmurundy hornblende diorite (analytical details are provided in Supplementary Electronic Materials).

6.2. Major oxides and trace elements

In this paper we present first full major and trace element data from several localities of igneous suites of the Itmurundy belt (Table 2; analytical details are provided in Supplementary Electronic Materials). The location of the sampling points is available in Table 1 and in Supplementary Fig. 1S made in Google Earth. The

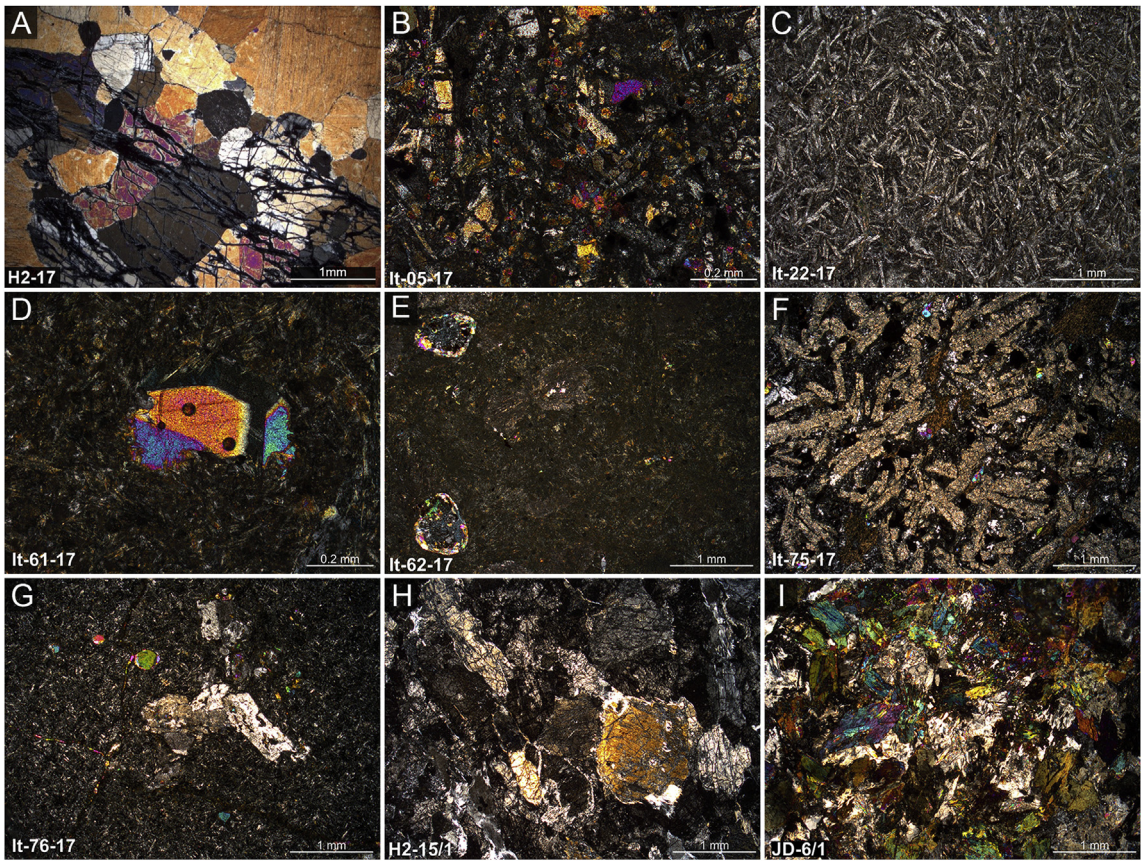

Fig. 8. Photos of thin sections of Itmurundy igneous rocks, central Kazakhstan. Description of samples see in Table 1.

geochemical data are illustrated in Figs. 10–13. The lavas and crystallized rocks from all localities are dominated by subalkaline varieties with several alkaline basalts, trachyandesites and phonotephrites: almost all samples plot in the basalt and basaltic andesite fields on the total alkalis ($K_2O + Na_2O$) vs. silica (SiO_2) classification diagram (Fig. 10A). As most of the volcanic rocks are associated with deep-marine sediments (see Section 2, Figs. 5 and 6) and therefore erupted in sub-marine conditions, they probably experienced strong sea-floor hydrothermal alteration. Accordingly, the concentrations of mobile elements, e.g., Rb, K, Na, Sr, Ba, Fe, and Pb, may have changed (e.g., Humphris and Thompston, 1978; Thompson, 1991; Valsami-Jones and Ragnarsdottir, 1997; Safonova et al., 2012). However, the SiO_2 vs. Nb/Y systematics based on relatively immobile elements also indicates alkaline basalt, subalkaline basalt and trachyandesite (Fig. 10B). All analyses presented in this paper have L.O.I. below 5% (Table 2). In evaluating which elements are suitable for geochemical interpretation in terms of their post-magmatic mobility we used the criteria discussed in our previous papers on oceanic basalts (e.g., Safonova et al., 2012, 2015).

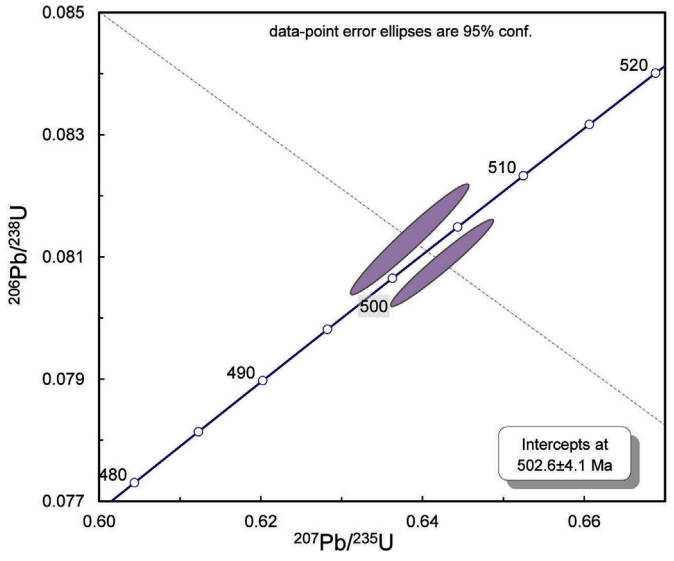

Fig. 9. U–Pb concordia plot of zircon grains from diorite in the western Itmurundy belt, central Kazakhstan.

The basaltic rocks possess low to high Mg# (cation proportion of $Mg/(Mg + Fe^{2+})$) ranging from 26 to 73, and MgO (1.8–9.4 wt.%) over a range of SiO_2 content from 44.1 to 55.1 wt.% (Table 2). The analyzed samples have low to high Ti, but most samples are within 1.5–3.4 wt.% TiO_2 and are characterized by variable Ca (4.9–16.9 wt.% CaO) and high Al (12.6–17.4 wt.% Al_2O_3) contents. In the $FeO^*/MgO - TiO_2$ diagram (Fig. 10C), the Itmurundy samples split in three groups, high-Ti and medium-Ti tholeiites and low-Ti island-arc varieties (Miyashiro, 1973). In the $FeO^*/MgO - FeO^*$ diagram we can recognize two major groups: higher Fe tholeiitic and lower Fe calc-alkaline (Fig. 10D). The diorite sample plots into the island-arc and calc-alkaline fields of the two diagrams, respectively. Most samples plot along a common trend in the MgO vs. major oxides diagrams (Fig. 11A–E), except for the samples plotted separately in the Miyashiro diagrams (Fig. 10C and D). The Al_2O_3/TiO_2 ratios in most samples are below 8 (Table 2), except for the low-Ti samples as seen in the MgO vs. major oxides and Miyashiro plots (Fig. 10C–D, 11A-E). Consequently, we can divide the samples

Table 2
Whole rock major oxides (wt.%) and trace elements (ppm) for Itmurundy igneous rocks, northern Balkhash.

	1	2	3	4	5	6	7	8	9	10	11	12	13
site	H1	H1	H1	H1	H1	H1	H2	H2	H2	H2	H2	H2	H2
rock	dolerite	basalt	basalt	basalt	basalt	basalt	dolerite	dolerite	basalt	gabbro	basalt	basalt	basalt
sample	IT-35-17	IT-36-17	IT-76-17	IT-77-17	IT-78-17	IT-79-17	IT-80-17	IT-05-17	IT-13-17	IT-16-17	IT-22-17	IT-43-17	IT-44-17
SiO_2	49.47	48.04	48.16	45.55	47.65	47.75	46.65	47.23	49.70	44.16	46.22	51.19	49.48
TiO_2	1.62	1.39	1.83	1.43	1.90	2.36	1.58	2.08	2.74	4.29	3.26	2.20	2.04
Al_2O_3	14.50	14.99	16.71	14.86	14.38	13.32	16.06	14.20	15.51	13.44	15.12	14.26	14.06
Fe_2O_3	11.49	10.08	14.89	12.57	12.43	14.10	11.19	12.00	12.12	16.65	14.46	11.36	10.12
MgO	7.20	8.34	4.00	9.38	6.94	6.97	7.71	6.74	3.07	5.58	3.09	6.97	5.41
CaO	10.66	7.87	6.12	8.82	11.03	9.32	9.21	9.94	5.38	7.49	5.52	6.33	10.11
MnO	0.20	0.16	0.14	0.18	0.19	0.22	0.17	0.25	0.15	0.17	0.10	0.15	0.15
Na_2O	2.52	3.15	4.61	2.63	3.08	2.82	2.78	2.38	4.88	2.69	2.72	3.61	4.49
K_2O	0.08	1.40	0.64	0.37	0.13	0.71	1.37	1.80	0.83	2.04	5.10	1.20	0.33
P_2O_5	0.15	0.12	0.22	0.12	0.17	0.22	0.13	0.22	1.16	0.41	0.83	0.27	0.25
LOI	2.51	4.62	2.47	3.25	2.71	2.77	2.85	2.96	4.74	2.47	3.68	2.83	4.00
Total	100.5	100.3	99.9	99.2	100.7	100.7	99.8	100.0	100.5	99.6	100.3	100.47	100.5
#Mg	61.3	57.4	64.1	62.8	63.4	67.9	58.2	62.8	61.0	71.2	65.7	61.4	59.0
Rb	0.6	27.4	10.7	5.5	1.7	12.6	19.0	20.2	6.1	19.2	57.7	14.4	2.9
Sr	327	245	254	277	308	262	262	483	224	432	184	121	162
Ba	40	210	104	45	21	74	111	772	689	562	773	182	44
Cs	0.1	0.7	0.4	0.3	0.3	0.2	0.2	0.1	0.2	0.5	0.5	0.2	<0.1
Y	30	38	40	37	38	64	28	30	49	26	45	37	35
Zr	108	97	118	102	113	184	97	143	545	196	420	151	148
Nb	4.4	2.1	5.6	4.6	6.0	9.4	4.4	12.3	73.3	42.1	62.3	10.4	11.4
La	5.8	3.8	7.2	4.9	6.6	9.7	4.6	12.4	60.1	35.1	54.4	10.0	8.5
Ce	15.8	11.1	18.4	13.7	16.9	26.7	12.4	29.1	125.3	69.0	109.1	25.0	21.9
Pr	2.6	2.0	2.8	2.3	2.8	4.4	2.0	4.2	17.2	8.5	14.5	3.7	3.5
Nd	13.1	10.9	13.7	12.6	13.7	22.1	9.7	19.1	69.7	33.5	58.3	18.3	16.3
Sm	3.7	3.8	4.7	3.9	4.3	7.1	3.4	4.8	14.2	6.9	12.2	5.2	4.9
Eu	1.4	1.2	1.7	1.5	1.7	2.3	1.2	1.7	4.8	2.2	3.2	1.8	1.6
Gd	4.7	5.2	5.7	5.4	5.7	9.4	4.3	5.5	13.6	6.7	11.4	6.1	5.5
Tb	0.9	0.9	1.0	0.9	1.0	1.6	0.8	0.9	1.9	0.9	1.7	1.0	1.0
Dy	5.5	6.5	6.7	6.1	6.8	10.6	4.8	5.6	10.4	5.4	8.9	6.8	6.6
Ho	1.1	1.3	1.5	1.3	1.4	2.2	1.0	1.2	1.9	1.0	1.7	1.3	1.3
Er	3.2	3.8	4.2	3.8	4.1	6.6	2.8	3.1	4.5	2.7	4.2	3.9	3.6
Tm	0.5	0.6	0.6	0.6	0.6	0.9	0.4	0.5	0.6	0.4	0.6	0.6	0.5
Yb	3.0	3.7	3.8	3.7	3.8	5.8	2.8	2.7	3.4	2.3	3.3	3.4	3.4
Lu	0.4	0.5	0.6	0.5	0.5	0.8	0.4	0.4	0.4	0.3	0.4	0.5	0.5
Hf	2.8	2.7	3.3	2.8	3.2	5.0	2.6	3.6	11.7	4.9	9.9	3.9	3.8
Ta	0.3	0.2	0.3	0.3	0.4	0.6	0.3	0.8	4.7	2.7	4.0	0.7	0.7
Th	0.3	0.2	0.4	0.4	0.5	0.8	0.4	1.1	10.5	3.7	9.3	0.8	0.9
U	0.2	0.2	0.2	0.2	0.2	0.3	0.1	0.6	1.9	1.0	1.8	0.4	0.8

	14	15	16	17	18	19	20	21	22	23	24	25	26	27
site	H2	H2	H2	H2	H2	H2	H2	H2	H2	H2	H2	OD1	OD1	NW
rock	basalt	basalt	basalt	basalt	basalt	gabbro	gabbro	basalt	gabbro	basalt	gabbro	gabbro	lava	diorite
sample	IT-60-17	IT-61-17	IT-62-17	IT-63-17	IT-64-17	IT-75-17	H2-15/1	N17008	IT-73-17	17081902	ИХ-14	H2-14	H2-16/1	JD6-1
SiO_2	53.52	53.64	49.27	52.26	54.19	48.88	49.59	54.52	51.93	49.29	52.30	48.12	48.20	55.11
TiO_2	2.90	2.25	2.92	2.87	2.55	2.66	2.45	2.57	0.95	1.57	0.17	0.40	0.25	0.58
Al_2O_3	14.26	14.21	14.76	14.12	15.16	15.80	17.37	13.48	14.51	12.61	14.86	15.41	17.54	14.46
Fe_2O_3	11.40	10.03	12.60	12.08	10.01	13.61	10.08	11.30	12.57	13.87	9.43	7.43	5.72	6.35
MgO	3.67	4.19	3.85	4.02	4.33	5.44	1.83	4.27	4.99	6.84	7.15	8.40	8.10	6.86
CaO	6.80	7.40	8.40	7.11	3.94	3.39	5.02	4.90	8.42	8.87	10.62	16.90	16.23	7.95
MnO	0.13	0.14	0.17	0.12	0.13	0.20	0.38	0.12	0.21	0.23	0.16	0.16	0.12	0.15
Na_2O	3.12	4.25	2.63	2.99	4.77	2.47	2.17	3.60	3.05	3.22	3.47	1.45	1.50	3.97
K_2O	1.47	0.77	2.61	2.13	0.89	2.51	6.85	0.86	2.62	1.19	0.11	0.10	0.38	2.08
P_2O_5	0.67	0.38	0.76	0.76	0.52	0.40	0.88	0.68	0.22	0.13	0.03	0.02	0.01	0.20
LOI	2.28	2.93	1.99	2.14	3.16	4.05	3.75	3.62	0.82	1.72	1.82	1.84	1.89	1.54
Total	100.4	100.3	100.1	100.8	99.8	99.54	100.5	100.0	100.4	99.7	100.2	100.3	100.0	99.4
#Mg	61.5	58.5	63.1	63.1	56.9	63.3	53.7	62.6	63.4	68.8	55.9	49.1	39.5	46.8
Rb	24.8	10.4	59.7	37.2	11.9	36.7	95.0	12.6	22.3	10.9	0.8	0.6	2.4	16.6
Sr	275	309	337	295	131	194	121	217	556	626	122	266	364	779
Ba	407	194	617	479	119	258	428	161	417	457	28	20	22	517
Cs	0.1	0.1	0.3	0.2	0.2	1.0	0.4	0.1	0.1	0.2	0.1	0.1	0.1	0.1
Y	38	25	41	39	37	39	38	35	22	39	6	9	7	14
Zr	336	185	397	417	363	266	275	389	55	98	20	7	5	71
Nb	31.6	20.2	33.9	31.9	46.9	30.7	60.6	30.1	1.9	2.5	1.1	0.4	0.2	13.0
La	34.9	20.6	38.0	34.7	40.1	29.6	53.9	31.6	8.9	8.4	1.6	0.6	0.4	16.7
Ce	69.1	40.9	76.1	70.9	80.9	63.7	101.8	65.2	20.4	16.9	3.0	1.6	0.9	32.3
Pr	9.2	5.6	10.1	9.4	10.8	8.2	11.8	8.7	3.1	2.4	0.4	0.3	0.2	4.2

(*continued on next page*)

Table 2 (*continued*)

	14	15	16	17	18	19	20	21	22	23	24	25	26	27
Nd	40.5	24.4	43.7	39.5	41.9	32.6	43.7	37.6	14.3	11.4	1.5	1.8	1.1	16.6
Sm	9.6	5.6	10.4	10.9	9.1	7.9	9.4	9.3	3.4	3.8	0.4	0.8	0.6	3.6
Eu	3.1	2.0	3.3	3.1	2.7	2.4	3.3	2.9	1.1	1.5	0.2	0.4	0.3	1.0
Gd	9.5	5.8	10.6	9.9	8.8	7.8	8.7	9.4	3.8	5.0	0.5	1.2	0.8	3.2
Tb	1.4	0.8	1.5	1.4	1.3	1.2	1.3	1.4	0.6	0.9	0.1	0.2	0.2	0.4
Dy	7.8	5.0	8.3	7.9	7.6	7.2	7.3	7.0	3.8	6.4	0.7	1.6	1.0	2.4
Ho	1.3	0.9	1.5	1.4	1.3	1.4	1.4	1.3	0.8	1.5	0.2	0.3	0.2	0.5
Er	3.6	2.3	4.0	3.6	3.4	4.0	4.0	3.5	2.2	4.2	0.6	1.0	0.7	1.4
Tm	0.5	0.3	0.5	0.5	0.5	0.6	0.6	0.5	0.3	0.6	0.1	0.1	0.1	0.2
Yb	2.8	1.8	3.2	2.9	3.0	3.6	3.7	2.7	2.0	4.1	0.7	0.9	0.7	1.2
Lu	0.4	0.3	0.4	0.4	0.5	0.5	0.5	0.4	0.3	0.6	0.1	0.1	0.1	0.2
Hf	8.0	4.5	9.5	9.5	8.6	6.3	6.2	9.0	1.6	2.8	0.6	0.3	0.2	2.1
Ta	2.2	1.4	2.3	2.0	3.2	2.0	3.8	2.0	0.1	0.2	0.1	0.05	0.05	0.6
Th	4.3	2.7	4.9	4.5	7.3	3.4	6.4	4.5	1.2	0.4	0.3	0.1	0.1	4.9
U	0.8	0.4	0.9	0.8	1.3	1.0	1.6	1.3	0.5	0.5	0.2	0.1	0.0	1.9

Abbreviations as in Table 1.

under study into three groups: high-Ti ($TiO_2 > 1.9$ wt.%; 14 samples), medium-Ti ($TiO_2 = 1.4–1.7$ wt.%; 7 samples) and low-Ti ($TiO_2 < 1.0$ wt.%; 5 samples) (Table 2). In the MgO vs. trace element plots (Fig. 11F-L), the high-Ti samples show the most distinct negative trends for all elements. The low-Ti samples are characterized by lower concentrations of most incompatible elements, e.g., La, Sm, Zr, Nb and Th, than the samples from other sites, and by two levels of Zr/Nb ratios at 7 and 34 (Fig. 11F, H, I, J, K; Table 2). The high-Ti samples have lower Zr/Nb ratios (20 in average) than the medium-Ti samples (24).

The chondrite-normalized rare-earth element (REE) patterns of the high-Ti samples (Fig. 12A) are typically slightly to strongly LREE-enriched ($La/Yb_n = 1.1–3.6$) and are characterized by differentiated HREE ($Gd/Yb_n = 1.3–3.2$) and low Zr/Nb ratios (4–14), resembling those of Hawaiian OIB. The REE patterns of the medium-Ti samples (Fig. 12B) are weakly LREE depleted to flat (La/

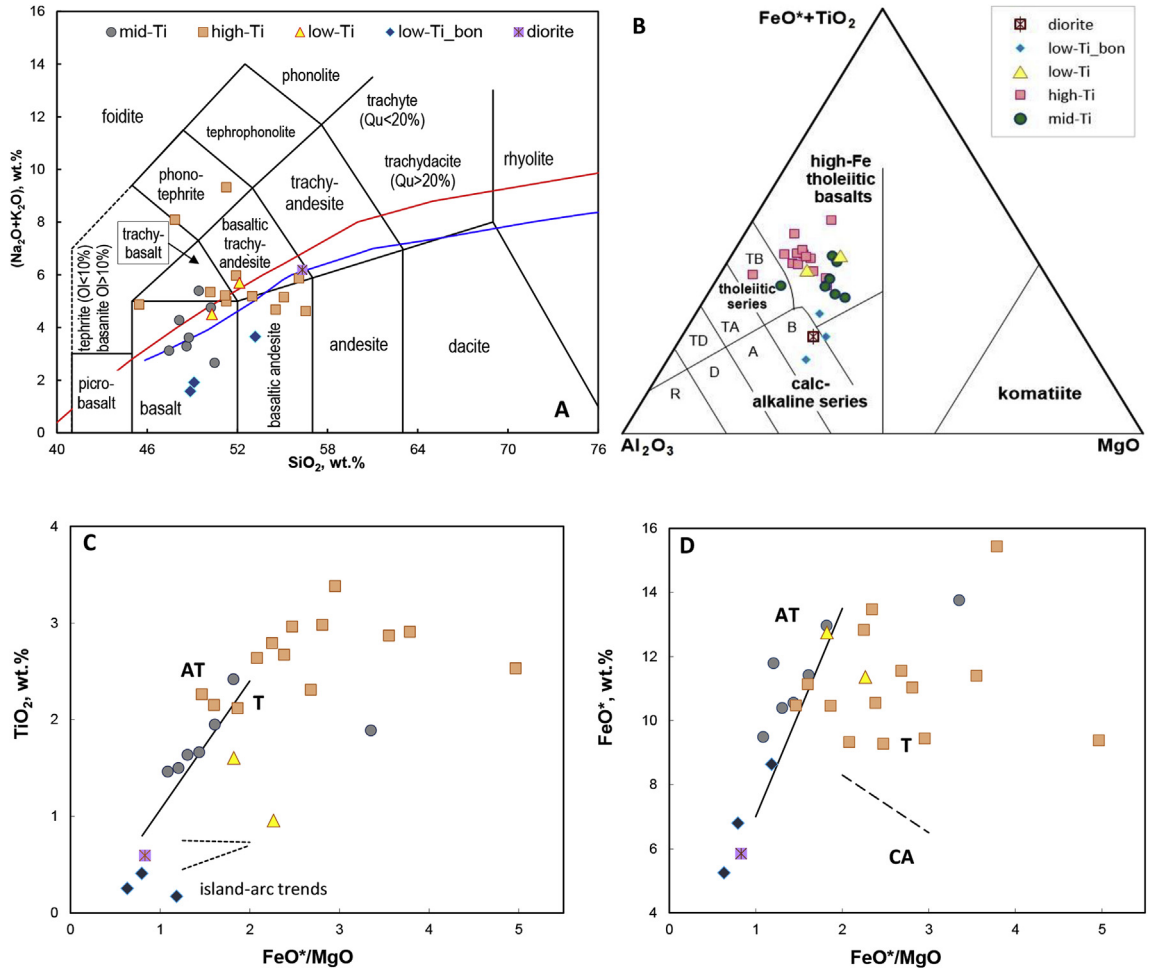

Fig. 10. Classification diagrams for igneous rocks of the Itmurundy belt, central Kazakhstan. A, SiO_2 – total alkali (Le Maitre et al., 2002); B, Al_2O_3–FeO^*+TiO_2–MgO diagram (Jensen, 1976); tholeiitic series: TA - andesite, TD - dacite, TR - rhyolite; calc-alkaline series: B – basalt, A - andesite, D - dacite, R – rhyolite. C, D, Miyashiro bivariant plots FeO^* - FeO^*/MgO (C); TiO_2 - FeO^*/MgO (D). Discriminant fields for abyssal tholeiite (AT), tholeiite (T) and calc-alkaline volcanic rocks (CA) are after (Miyashiro, 1973).

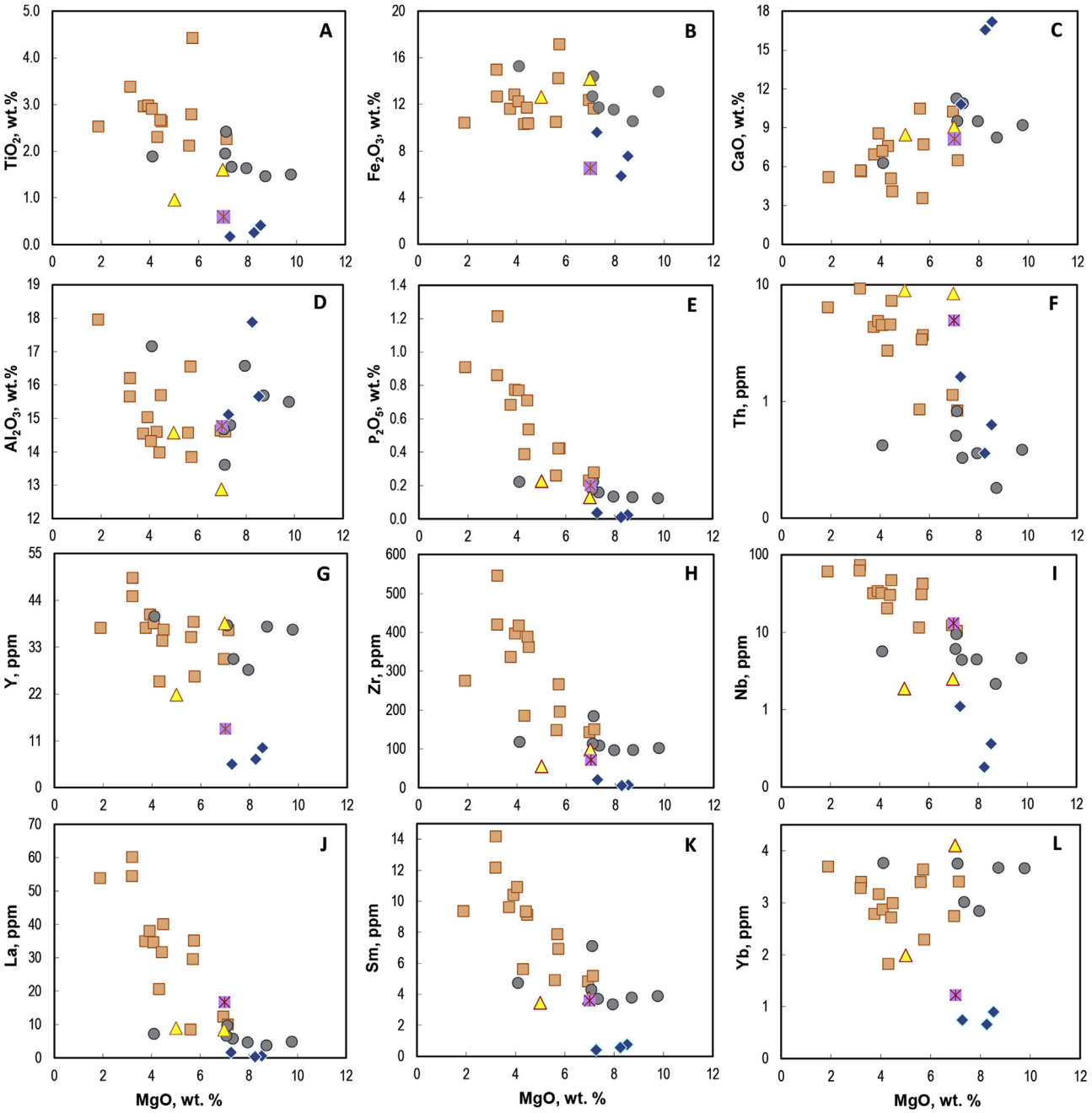

Fig. 11. MgO vs. major oxides (A–E) and trace elements (F–L) of volcanic and subvolcanic rocks of the of the Itmurundy belt, central Kazakhstan. Symbols as in Fig. 10.

$Yb_n = 0.8–1.0$) and show no notable HREE differentiation ($Gd/Yb_n = 1.1–1.3$). The low-Ti samples possess total REE similar to those of the medium-Ti samples and lower and they show variable REE patterns (Fig. 12C and D). In general, the REE patterns of the low-Tigroup are flat to LREE-depleted or slightly LREE enriched ($La/Yb_n = 0.4–1.4$; $Gd/Yb_n = 0.6–1.7$). One subgroup shows flat to slightly differentiated REE patterns (Fig. 12C). Another subgroup (boninite-type) have LREE depleted to LREE enriched patterns with not differentiated HREE (Fig. 12D). The low-Ti diorite sample (Fig. 12E) is LREE enriched and show differentiated HREE ($La/Yb_n = 2.9$; $Gd/Yb_n = 2.0$). Most samples show zero to weak Eu anomalies (Fig. 12A–E).

The primitive mantle normalized multi-component spectra for the most of the high-Ti samples are characterized by positive Nb anomalies relative to La and, to a lesser degree, Th ($Nb/La_{pm} = 1.2$; $Nb/Th_{pm} = 1.0$ in average; Table 2; Fig. 12F), which are typical of many accreted OIB-type basalts (e.g., Polat et al., 1999; Ichiyama et al., 2008; Safonova and Santosh, 2014; Safonova et al., 2015). The medium-Ti samples display no notable Nb enrichment relative to La, but strong enrichment in respect to Th ($Nb/La_{pm} = 1.0$, $Nb/Th_{pm} = 1.5$ in average; Table 2; Fig. 12G), that is more typical of MORB. The multi-element spectra for the low-Ti samples (Fig. 12H–J) possess clear Nb depletion relative to Th and La ($Nb/La_{pm} = 0.45$; $Nb/Th_{pm} = 0.4$ in average; Table 2). The presence of Nb troughs is a typical feature of rocks formed in supra-subduction settings. Several basalts from site Horse-2 and the gabbro-diorite JD6-1 (Table 2) are characterized by Zr peaks in the multi-element spectra. The content of Th in the high-Ti samples ranges from 1 to 10 (4.6 in average), which is close to typical OIB (4 ppm; Sun and McDonough, 1989) and higher than in the middle-Ti

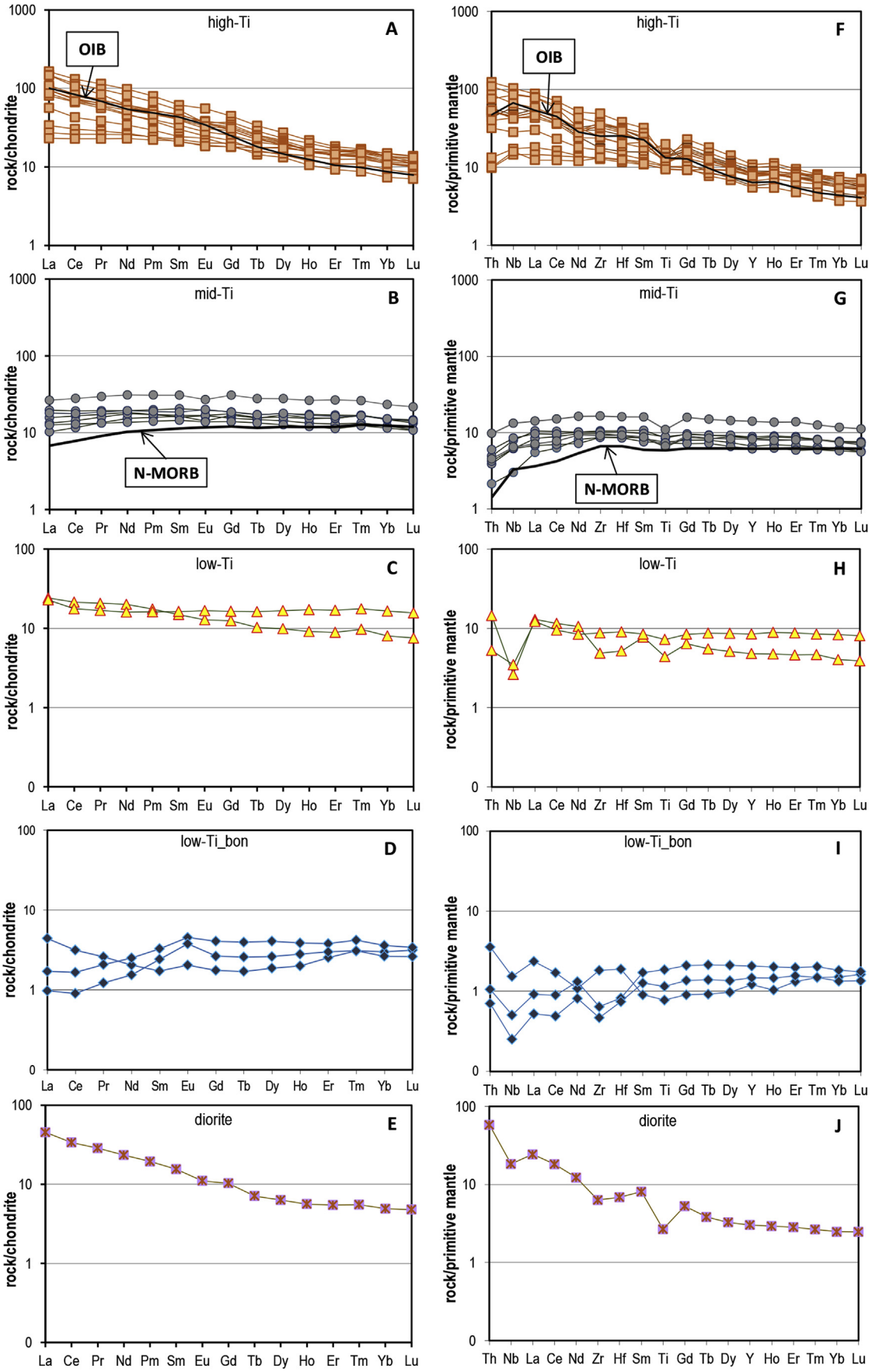

Fig. 12. Chondrite-normalized rare-earth element patterns (A–E) and primitive mantle-normalized multi-component trace element patterns (spidergrams; F-J) for of volcanic and subvolcanic rocks of the of the Itmurundy belt, central Kazakhstan. Normalization values are from Sun and McDonough (1989).

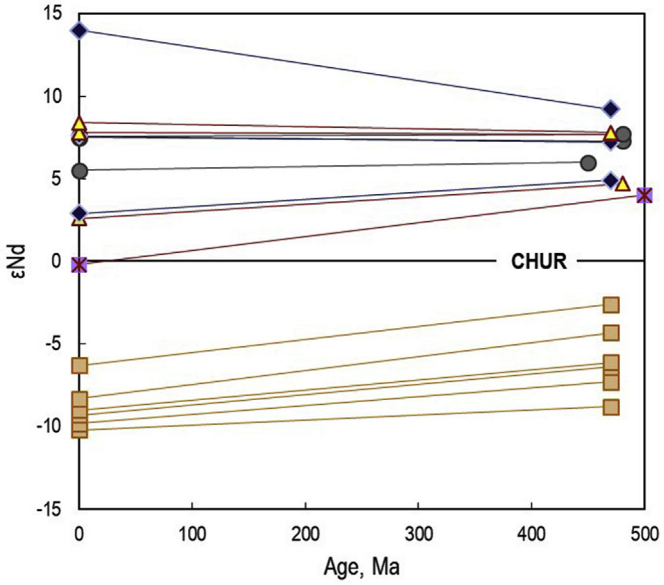

Fig. 13. Epsilon Nd(t) versus age plot for volcanic and subvolcanic rocks of the Itmurundy belt, central Kazakhstan. Symbols as in Fig. 10.

samples (0.2–0.8). A part of samples of all groups display negative Ti anomalies in the multi-element spectra (Fig. 12F–J). Thus, based on the concentrations of major and trace elements we conclude that the high-Ti samples are enriched in LREE and Nb that is typical of OIB-type or plume-type basalts (e.g., Sun and McDonough, 1989; Hofmann, 1997; Regelous et al., 2003; Safonova and Santosh, 2014; Safonova et al., 2012, 2015, Table 2; Fig. 11F-L, 12A, F). The medium-Ti samples are geochemically similar to MORB (Fig. 12B, G). The low-Ti samples possess geochemical features more characteristic of volcanic and subvolcanic rocks formed in supra-subduction settings. A part of the low-Ti samples represent basaltic boninites, i.e. they are enriched in MgO (7.2–8.4 wt.%), depleted in all REE and are characterized by the lowest Nb negative anomalies, suggesting their intra-oceanic arc origin.

6.3. Whole rock Nd isotopes

We present first Nd isotope data from igneous rocks of the Itmurundy belt in central Kazakhstan (analytical details are provided in Supplementary Electronic Materials). The initial isotopic ratios were calculated to late Cambrian-Ordovician ages based on biostratigraphic data (Zhylkaidarov, 1998; Nikitin, 2002; Safonova et al., 2019) or U–Pb zircon ages (section 6.1). The low-Ti diorite was calculated to 490 Ma (section 6.1). The medium-Ti samples (geochemically close to MORB) were calculated to 470 Ma, which is the average age of associated Ordovician chert (section 3). The high-Ti samples (close to OIB) were calculated to 450 Ma as oceanic islands may be coeval or younger than associated MORBs. We interpret the compositional range of Nd isotope data in terms of different sources characterized by different isotope signatures and possible fractionation between the parent and daughter isotopes during later low-grade metamorphism, which may have affected in particular those samples with abundant secondary minerals (Romer et al., 2005). The samples have both positive and negative εNd(t) values (Table 3). The medium- and low-Ti samples have higher $^{143}Nd/^{144}Nd$ (0.5128–0.5134), whereas the high-Ti samples have lower $^{143}Nd/^{144}Nd$ (0.5121–0.5123) (Table 3). The εNd(t) values suggest that the igneous rocks were derived from two major kinds of sources: the growth lines for a part of samples are almost horizontal as typical of mantle rocks and there are both positive and negative εNd(t) groups (Fig. 13). The positive εNd(t) group includes the medium-Ti samples (εNd(t) ranging from 4.7 to 7.7) and low-Ti samples (εNd(t) ranging from 4.9 to 9.2), i.e. the rocks, which likely formed at mid-oceanic ridges and at intra-oceanic island arcs. The negative εNd(t) group includes the high-Ti samples (εNd(t) ranging from −4.3 to −8.8) probably reflecting an enriched mantle source. In addition, taken into consideration that the high-Ti samples show high degree secondary alteration, we may suggest that the shift of εNd(t) to the negative values could be caused by the fractionation between the parent and daughter Nd isotopes during sea-floor hydrothermal metamorphism and accretion-collision related greenschist metamorphism.

7. Discussion

7.1. Petrogenesis and mantle sources of the Itmurundy igneous rocks

The wide variations of MgO within the high-Ti and medium-Ti groups of samples (Fig. 11) and the presence of phenocrysts in some but not other samples (Fig. 8) suggest fractional crystallization. The absence of notable Eu anomalies in most samples excludes significant plagioclase fractionation (Fig. 12A–E). Fractionation of Ti–Fe oxides can be proposed for some of the samples because the medium-Ti samples and a part of high-Ti and low-Ti samples show negative Nb and Ti anomalies in the multi-element spectra (Fig. 12G–J). The generally negative trends in the MgO vs. TiO_2 plots and the absence of depletion in Nb are typical of the high-Ti samples (Figs. 11A and 12F) indicate that fractionation of oxide minerals in most OIB-type lavas played no major role. The stable Al_2O_3/TiO_2 ratios in the mid-Ti and high-Ti samples may reflect a similar mantle source composition, but the variable Gd/Yb_n ratios suggest variable degrees of partial melting of such a source (Table 2; Fig. 14A). The medium-Ti samples have higher Zr/Nb ratios (Table 2), lower concentrations of TiO_2 and Nb (Fig. 11A, J) and slightly higher Al_2O_3/TiO_2 ratios at nearly equal Gd/Yb_N ratios compared to a part of the high-Ti samples (Fig. 14A). As distinct from the high-Ti and mid-Ti samples, the negative anomalies of Ti and Nb in the multi-element spectra of the low-Ti samples (Fig. 12H–I), titanomagnetite in thin sections (Fig. 9, section 5) and variable Al_2O_3/TiO_2 ratios (Fig. 14A) suggest fractionation of Ti–Fe oxides during crystallization of their parent melts. The high-Ti samples show better defined trends in most plots (compared to other samples) suggesting fractionation of pyroxene and plagioclase (Fig. 11).

In terms of mantle sources, all high-Ti samples possess REE spectra with significantly differentiated HREE (Table 2; Fig. 12A, F). In the Gd/Yb_N vs. Al_2O_3/TiO_2 diagram, the high-Ti varieties with negative εNd (section 7.3, Table 3) plot in the field of Hawaii OIB (Fig. 14A) suggesting their derivation from enriched mantle sources, i.e. different from the one that produced the medium- and low-Ti rocks. In the Sm/Yb_n vs. Nb/La_n diagram (Fig. 14B), they define a group with similar Nb/La_n ratios suggesting variable degree of melting of, as inferred from isotope data, an enriched mantle source, which is typical of OIB-lavas hosted by accretionary complexes of Asia (Safonova and Santosh, 2014; Safonova et al., 2011, 2012, 2015). The medium-Ti samples encompass the compositional range of MORB, which, coupled with positive εNd (Table 3), suggests a different mantle source. The low-Ti samples possess highly positive εNd (Table 3, Fig. 13) and plot close to back-arc basin and intra-oceanic arc basalts in the REE and trace element plots (Figs. 12 and 14) suggesting their formation in an intra-oceanic arc. More evidence for such a origin comes from other coeval intra-oceanic arc terranes, which have been also recognized in central Kazakhstan, for example, the Late Cambrian-Early Ordovician Bozshakol-Chingiz arc (gray field in Fig. 1) (Degtyarev, 2011; 2012;

Table 3
Whole-rock Nd isotope data from Itmurundy igneous rocks.

	sample	Rock type	Group	age, Ma	Sm	Nd	Sm^{147}/Nd^{144}	Nd^{143}/Nd^{144}	Err	ε_{Nd} (0)	ε_{Nd}(T)
1	IT-61-17	porphyric basalt	high-Ti	470	6.05	23.67	0.1546	0.512134	10	−9.8	−7.3
2	IT-62-17	porphyric basalt	high-Ti	470	10.34	41.85	0.1494	0.512163	14	−9.3	−6.4
3	IT-63-17	aphyric basalt	high-Ti	470	10.60	43.27	0.1480	0.512178	7	−9.0	−6.1
4	IT-64-17	aphyric basalt	high-Ti	470	9.21	43.11	0.1291	0.512211	10	−8.3	−4.3
5	IT-22-17	aphyric basalt	high-Ti	470	13.26	59.15	0.1355	0.512316	6	−6.3	−2.6
6	IT-35-17	dolerite	mid-Ti	450	3.94	12.62	0.1886	0.512921	8	5.5	6.0
7	IT-76-17	porphyric basalt	mid-Ti	480	5.14	15.53	0.1998	0.513022	8	7.5	7.3
8	IT-79-17	aphyric basalt	mid-Ti	480	5.42	16.76	0.1955	0.513026	7	7.6	7.7
9	IT-80-17	gabbro-dolerite	mid-Ti	480	4.15	12.37	0.2026	0.513027	18	7.6	7.2
10	IT-73-17	microgabbro	low-Ti	480	3.69	13.63	0.1636	0.512773	5	2.6	4.7
11	17081902	aphyric basalt	low-Ti	470	3.75	10.93	0.2072	0.513069	8	8.4	7.8
12	H2-14	gabbro	low-Ti	470	0.51	1.53	0.2000	0.513040	10	7.8	7.7
13	H2-16/1	microgabbro	low-Ti	470	0.45	0.97	0.2768	0.513355	14	14.0	9.2
14	ИХ-14	microgabbro	low-Ti	470	0.34	1.24	0.1651	0.512789	19	2.9	4.9
15	JD-6/1	diorite	low-Ti	500	3.36	17.36	0.1309	0.512630	7	−0.2	4.0

For sample details see Table 1.

Safonova et al., 2017). The Bozshakol volcanic (tholeiitic and calc-alkaline series) and plutonic (tonalite) rocks show high whole-rock εNd(t) values (+5.4 to +17.0; Shen et al., 2007). Two intra-oceanic arcs of Middle Devonian and early Carboniferous age have been identified in eastern Kazakhstan, which basaltic to andesitic volcanic also yielded positive whole-rock εNd(t) values (+2.9 to +8.8; Safonova et al., 2018).

The diorite is compositionally close to the rocks of probably supra-subduction origin (Figs. 10C and 11F, L). On the other hand, in many diagrams plot also close to mid-ocean ridge varieties (Figs. 10D and 11A-K). The REE curve of diorite JD6-1 is close to OIB (Fig. 12E), but the multi-element curve shows Nb depletion relative Th and La (Fig. 12J).

7.2. Tectonic implications for the Itmurundy igneous rocks

The geochemical and isotope composition of the Itmurundy volcanic, subvolcanic and plutonic rocks suggest their formation in different tectonic settings. The high-Ti rocks suggest their eruption at oceanic islands of the Paleo-Asian Ocean similar to those of the Emperor-Hawaii chain of seamounts and volcanoes probably related to the Pacific hot spot or mantle plume (e.g., Regelous et al., 2003; Safonova et al., 2011, 2015; 2016; Safonova and Santosh, 2014; Yang et al., 2015). The medium-Ti samples probably formed in a mid-oceanic ridge tectonic setting and represent typical oceanic floor basalts present at the base of OPS. The low-Ti volcanic and subvolcanic rocks formed in a supra-subduction setting. The diorite, which yielded the age of ca. 500 Ma, occurs as a fragment in serpentinite mélange (section 2) and possesses gabbro-like petrography with many grains of normal hornblende instead of clinopyroxene (Fig. 8I). The ca. 500 Ma ages of the diorite are the first data from this area corresponding to the age of supra-subduction magmatism. These features, the composition and the 500 Ma age of the diorite, which is older than the age of the Itmurundy OPS (Ordovician-early Silurian; section 2, 3), allow us to suggest that sample was a part of the ophiolite section, probably supra-subduction ophiolite, which formation (later Cambrian) started a bit earlier than the OPS sedimentation began (early Ordovician).

In the geological map (Koshkin and Galitsky, 1960, Fig. 2) the volcanic rocks are all shown within the Itmurundy Fm. However, our data clearly indicate that they formed in different tectonic settings, oceanic (mid-oceanic ridge and oceanic island) and supra-subduction. Thus, we propose that the stratigraphic subdivisions in this region must be re-considered.

7.3. Itmurundy OPS lithologies

The lithology and composition of the rocks of the Itmurundy orogenic assemblage fit pretty well the model of Ocean Plate

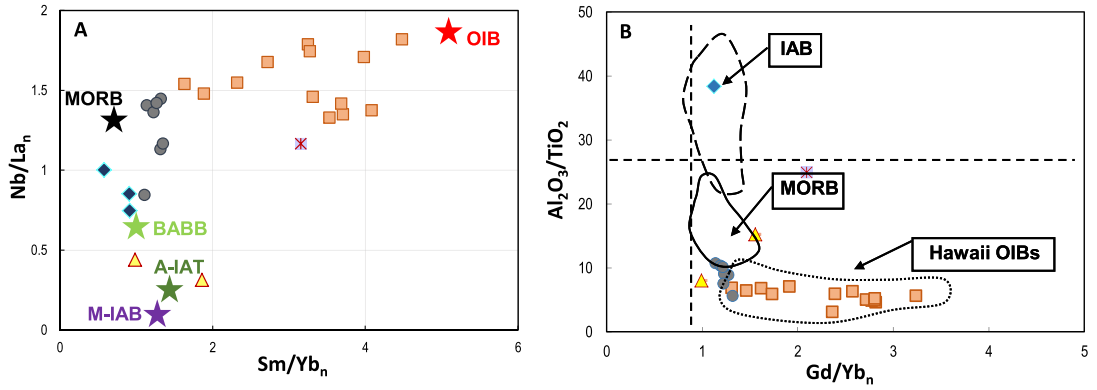

Fig. 14. Gd/Yb_n vs. Al_2O_3/TiO_2 (A) and Sm/Yb_N vs. Nb/La_{pm} (B) binary diagrams illustrating mantle sources of volcanic and subvolcanic rocks of the Itmurundy belt, central Kazakhstan. IAB – island-arc basalt; MORB – mid-oceanic ridge basalt; OIB – ocean island basalt. The average compositions (stars) of back-arc basin basalts (BABB), Aleutian arc tholeiites (A-IAT) and Mariana arc basalts (M-IAB) are from the GEOROC database (www.georoc. mpch-mainz. gwdg.de/georoc). OIB and MORB – from (Sun and McDonough, 1989). Symbols as in Fig. 10.

Stratigraphy - OPS (e.g., Isozaki et al., 1990; Maruyama et al., 2010; Safonova et al., 2016). OPS represents a regular and lithologically persistent succession of igneous (mostly basalts) and sedimentary rocks of (Fig. 15), which, respectively, erupted or deposited on the oceanic floor while the oceanic lithosphere was travelling from mid-oceanic ridge towards subduction zone. The OPS succession consists of (from bottom to top) ocean floor basalts, pelagic chert, hemipelagic siliceous mudstone, siltstone and shale, trench turbidite and conglomerate. When approaching the trench, the rocks of the subducting oceanic plate are scrapped off the surface and get attached or accreted to island arcs (Japan, Philippines, Indonesia) or active continental margins (Chile, Alaska). In addition, to ocean floor and trench facies, the model of OPS includes volcanic rocks and sediments formed at intra-oceanic rises, such as oceanic islands (Hawaii Chain), seamounts (Emperor Chain) and plateaus (Ontong-Java). The seamount OPS consists of main basaltic body capped by carbonates (island/seamount top), clastic rocks (slope facies) and oceanic sediments (foothill facies). The main volcanic body consists of oceanic island basalts (OIB-type) and oceanic plateau basalts (OPB-type) (Neal et al., 1997; Regelous et al., 2003). The top shallow-water carbonates are typically massive/micritic/reefal limestone, which form around an oceanic island (atoll) or on its top, when the island submerges under water after the cessation of volcanism. The slope facies are dominated by carbonate-volcanogenic epiclastic rocks showing syn-sedimentation folding (Z-folds) or slump bedding, brecciation and uneven thickness of sedimentary beds and volcanic flows. The seamount/island foothill facies include oceanic hemipelagic sediments (siliceous mudstone and siltstone often carbonaceous, clastic limestone, etc.) and pelagic sediments (chert). Oceanic island and seamounts represent topographic highs on the oceanic floor and therefore the seamount OPS is usually better accreted and preserved on the surface than the "standard" OPS (MORB-chert-mudstone), which units are subducted together with the oceanic lithosphere (Safonova and Santosh, 2014).

The rocks of the Itmurundy accretionary complex include most types of OPS rocks: MORB-type and OIB-type basalts (section 7) overlapped by pelagic chert and hemipelagic sediments (sections 2, 3) (Fig. 15). The Itmurundy sediments are often deformed and asymmetrically folded as a result of accretion and later oceanic suturing resulting in almost vertical dipping. During accretion, the detached packages consisting of pelagic and hemipelagic sediments, in places, underlain by basalt, could be vertically piled over each other to form "duplex" structures, which are observed in many places of the Itmurundy accretionary complex (section 4; Figs. 3 and 6).

There are no carbonate cap facies in the Itmurundy belt though, which could be expected in association with OIB-type basalts (Safonova and Santosh, 2014; Safonova et al., 2015). This suggests that either the Itmurundy seamounts did not reach the carbonate compensation depths, or that their travel from the point, where the volcanism stopped, to the subduction zone was rather long and the carbonates were dissolved. A similar situation was recorded in the Zasur'ya accretionary complex of the Russian Altai, which hosts late Cambrian-early Ordovician OPS also dominated by thick pelagic sediments but no carbonates (Safonova et al., 2011).

The greywacke-like sandstones are not thick in Itmurundy; the thickness of sandstones exposed at several outcrops is several meters in the central part of the belt, but increases to 10–15 m in its south-eastern part (Figs. 2 and 7). The small thickness of the

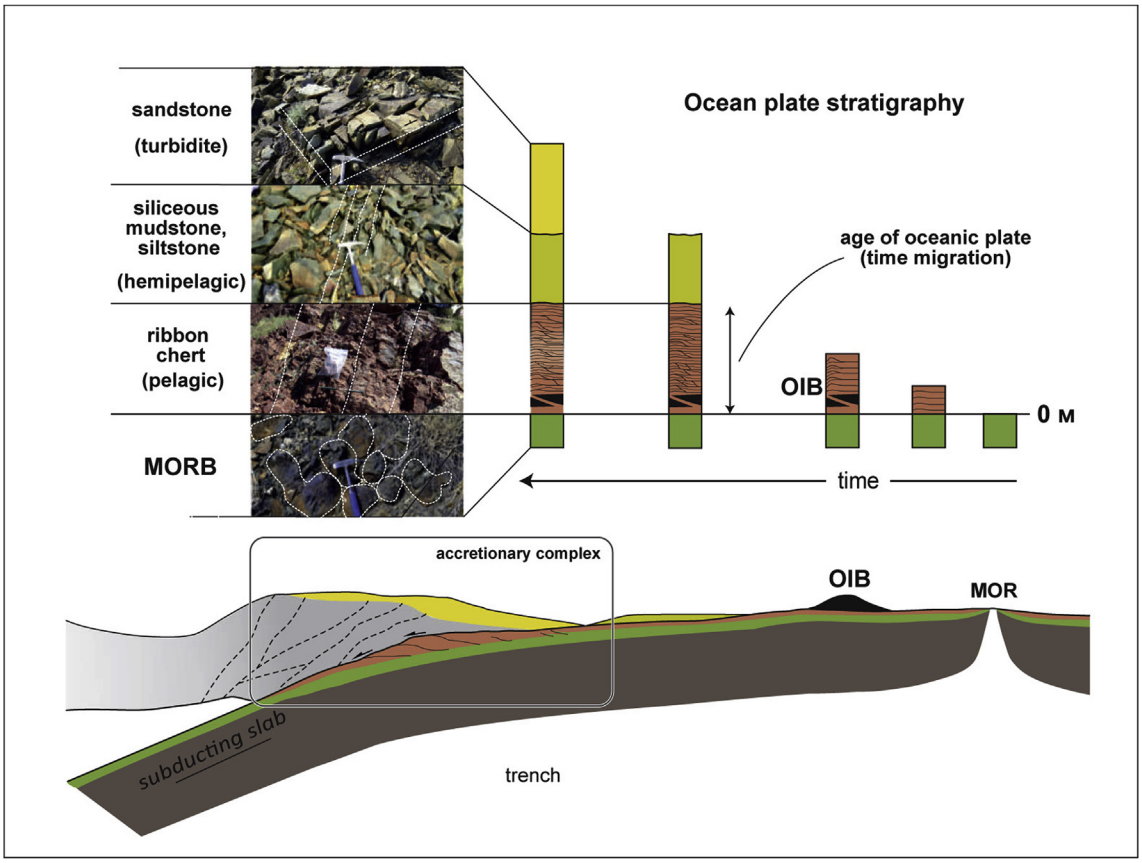

Fig. 15. A cartoon of Ocean Plate Stratigraphy (OPS) and formation of an accretionary complex illustrated by photos from the Itmurundy accretionary complex, central Kazakhstan (modified from Maruyama et al., 2010).

sandstones suggests either their tectonic erosion and subduction, or a small/thin volcanic arc, from which they were derived (Fig. 16). More details on the composition and age of the Itmurundy sandstones will come in the next paper on the Itmurundy belt.

7.4. Pacific-type nature of the Itmurundy belt

Based on the previous and our new data we conclude that the Itmurundy zone represents a Pacific-type orogenic belt. It has been widely accepted that a Pacific-type orogenic belt consists of three major parts: (1) intra-oceanic arc, i.e. island arc separated from continent by back-arc basin; (2) blueschist belt formed after MORB, OIB and OPB; (3) accreted OPS units (e.g., Dewey and Bird, 1970; Matsuda and Uyeda, 1971; Maruyama et al., 1996; Maruyama et al., 1997; Yarmolyuk et al., 2013; Safonova and Maruyama, 2014; Safonova, 2017; Safonova et al., 2017). Evidence for this comes from the following observations and published and original data.

(1) The idea of an intra-oceanic arc was first proposed in (Kurenkov et al., 2002) based of lithological and paleomagnetic data. Our new data show that the orogenic association of the Itmurundy zone includes igneous rocks with supra-subduction geochemical characteristics (section 6.2) and greywacke sandstones (section 2, Safonova et al., 2019; more to come in the second paper on Itmurundy). Moreover, a part of the volcanic rocks possess compositions close to the boninite series (Table 2; section 6.2, Fig. 11A, E, H, K, 12D, I) and strongly positive epsilon Nd values from +7.7 to +9.2 (Table 3; section 6.3). These data allow us to suggest that an Ordovician intra-oceanic arc once existed at an active margin of the Paleo-Asian Ocean.

(2) Several early publications mentioned blueschists formed after oceanic basalts, amphibolites with omphacite, garnet and rutile, i.e. formed after eclogites, and other high-pressure metamorphic rocks of early-middle Ordovician age (Antonyuk, 1974; Avdeev, 1986; Ermolov et al., 1990; Ermolov, 2008). Those metamorphic rocks were protoliths of famous Itmurundy jadeites as the Itmurundy zone hosts a large jadeite deposi (Ermolov et al., 1990; Kovalenko et al., 1994).

(3) The major features of the Itmurundy orogenic association are accreted OPS units. The Itmurundy zone includes all types of OPS: MORB to OIB oceanic basalts (section 6.2) often as pillow-lavas (sections 3, 5; Figs. 5A and 15) overlapped by pelagic and hemipelagic siliceous sediments of the Itmurundy Fm. (chert, siliceous mudstone; section 4), thick variably colored ribbon cherts, siliceous mudstones, siltstones and shales of the Kazyk Fm. and siliceous fine-grained clastic and sandstones of the Tyuretai Fm (sections 2, 3, 7.1; Figs. 4 and 15). Although the geological survey subdivided these rocks into three separate formations (Itmurundy, Kazyk, and Tyuretai; Koshkin and Galitsky, 1960; Patalakha and Belyi, 1981), de-facto all of them represent different segments of an OPS section (basalt-pelagic chert, pelagic-hemipelagic sediments, hemipelagic-trench-forearc sediments, respectively), i.e. poorly preserved fragments of one oceanic plate, which once existed in an Ordovician-early Silurian ocean (Fig. 16).

7.5. Tectonic history of the Itmurundy zone

As follows from the previous section, the Itmurundy zone represents a Pacific-type orogenic belt, similar to those of the western Pacific (Japan, Indonesia, etc.), hosting fragments of intra-oceanic arc(s), high-pressure metamorphic rocks (eclogite? blueschist) and OPS rocks. The identification of OPS units is of crucial importance, because accretionary prisms possess very complicated structures (Wakita, 2012) making their investigation and stratigraphic reconstruction hardly problematic. The complicated structure of an accretionary prism forms during accretion, when the “MORB-chert-shale” sequences detached from the subducting oceanic plate can be vertically piled over each other or thrust under each other to form “duplex” structures, in which the older units may appear on the top (Maruyama et al., 2010; Wakita, 2012; Safonova et al., 2019, Figs. 3B, 7 and 15). The OPS model coupled with careful geochronological dating of each package would allow recognizing those inconsistencies and reconstructing the accreted units and the sense of subduction correctly. Therefore, the careful study of relationships between various OPS rocks is a reliable method for the understanding of the present structure and the past history of accretionary complexes and their hosting P-type orogenic belts.

Accreted OPS units often form duplex structures consisting of lithologically uniform horses (basalt-chert-siliceous mudstone or chert-siliceous mudstone, etc.). The Itmurundy duplex structures form by the thrusting of horses under each other along a lower detachment surface (bottom thrust), so that younger horses appear under older (Fig. 3B). The bottom thrusts can be identified by the OPS lowest basaltic package of the Itmurundy Fm. The duplex deformation features of the central part of the Itmurundy zone (segment V) strongly indicate the SE to NW sense of subduction (in

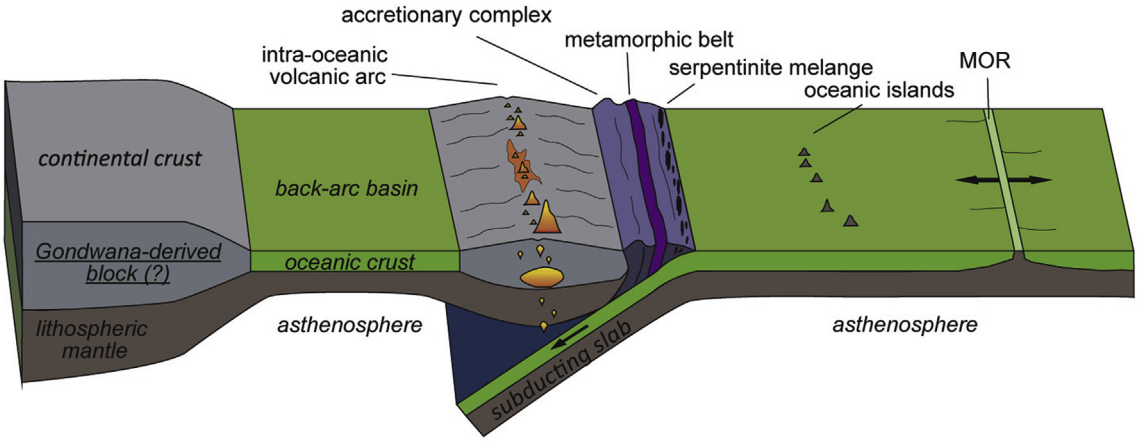

Fig. 16. A scheme of the formation of the Itmurundy Pacific-type orogenic belt including ophiolites, OPS incorporated into the accretionary complex and an intra-oceanic arc.

present coordinates), which is also consistent with the stratigraphic top facing to the SE (Fig. 3). The later post-orogenic deformations characterize the northeastward compression, which resulted in the anticline folding of the eastern duplex (Fig. 7) and in the activation of the duplex thrusts separating segments I-III, IV-VIII and VIII. The ultramafic serpentinized rocks possibly extruded at that compressional stage. Moreover, the active processes of accretion along an intra-oceanic arc (section 7.4; Fig. 3) was paired with active supra-subduction magmatism forming a typical Pacific-type orogenic belt during Cambrian-Ordovician time (Fig. 16).

In terms of determining the sense of subduction we must take into account that the Itmurundy zone is located in the core of the Kazakh orocline (Fig. 1) and therefore in Ordovician time the arc was not bended but extended along an active margin of a terrane or microcontinent probably split off East Gondwana (Mossakovsky et al., 1993; Buslov et al., 2001; Windley et al., 2007).

According to the geological maps of (Patalakha and Belyi, 1981) and our field observations (Figs. 2, 3 and 5B), the thickness of the red and brown ribbon cherts seems to be of an order of 200 m. Assuming a rate of sedimentation in deep-sea conditions at 1–3 mm per one thousand years (Isozaki et al., 1990; Hori, 1992; Safonova et al., 2016), the lifetime of chert deposition could be ca. 150 Ma or even longer. This suggests that the Itmurundy oceanic realm was not a relatively small back-arc or marginal basin (Stepanets, 2016) but rather a big ocean (Fig. 16).

Based on the previous and new data we may propose the following scenario for the formation of the Itmurundy zone at northern Bakhash. The Itmurundy belt probably developed in two major stages: Caledonian (early Paleozoic) and Hercynian (late Paleozoic). During the Caledonian stage, the ophiolites were formed and emplaced by thrusting or wedge extrusion (Maruyama et al., 2011). The Hercynian folding and blocky deformation formed serpentinite and induced schistosity and boudinage. The faunal assemblages, which were recovered from the pelagic oceanic sediments (section 3), are coeval with the Early-Middle Ordovician conodonts from the shelf deposits of southern Kazakhstan (Zhylkaidarov, 1998). However, the shallow-water assemblages of hemipelagic sediments are taxonomically more diverse and the warm-water forms constitute approximately half of the amount of specimen. This corroborates the idea that the Ordovician active margins around the Paleo-Asian Ocean, which later merged to form the Kazakhstan continent, were closer to the equator than to the Baltic region (Scotese and McKerrow, 1991; Windley et al., 2007). The latest Cambrian to early Silurian intra-oceanic arc(s) finally collided with continental margins and/or a composite continent located to the north to contribute to the formation of much larger ca. 2000 km long Kazakhstan megablock of triangular shape by mid-Silurian time (e.g., Windley et al., 2007; Degtyarev, 2012; Safonova et al., 2017). The more than 100 m thick pelagic sediments indicate the existence of a wide ocean in the early Paleozoic, which size can be compared with that of the modern Pacific Ocean, rather than a back-arc basin (Fig. 16).

8. Conclusions

The Itmurundy zone of northern Balkhash consists of three rock associations: mantle (ultramafic-mafic rocks, serpentinite mélange), orogenic (accretionary and supra-subduction complexes) and post-orogenic (continental deposits). Diorite from serpentinite mélange yielded a U–Pb age of ca. 500 Ma. The orogenic association includes the rocks of three formations: Itmurundy (O_{1-2}), Kazyk (O_{2-3}) and Tyuretai (O_3–S_1). The geological relationships and lithologies of these three formations fit the model of Ocean Plate Stratigraphy: basalt – pelagic chert – hemipelagic siliceous mudstone and siltstone – trench/forearc sandstone. Both the igneous and sedimentary rocks are strongly folded, sheared and greenschist metamorphosed and often occur as duplex structures consisting of basalt-chert and/or chert-siliceous mudstone horses.

The mafic igneous rocks (aphyric and porphyric basalts, dolerite, microgabbro) are most typical of the Itmurundy Fm. There are three main types of rocks: high-Ti, medium-Ti and low-Ti possessing different major and trace element and Nd isotope characteristics. The high-Ti rocks are associated with volcanogenic-sedimentary breccias and hemipelagic sediments, they possess geochemical affinities of OIB and probably erupted in an intra-plate oceanic setting, i.e. on oceanic islands related to mantle plume activity. The medium-Ti samples are compositionally similar to MORB; they occur in contact with pelagic chert and therefore formed in a mid-oceanic ridge tectonic setting. The low-Ti volcanic and subvolcanic rocks show geochemical features close to those of island arc tholeiites and boninites and probably formed in a supra-subduction setting, at an intra-oceanic arc.

The Itmurundy belt represents a typical Pacific-type belt as it includes accreted OPS units, metamorphic rocks (blueschist, eclogite), and intra-oceanic arc units. The more than 100 m thickness of pelagic ribbon chert suggests that the Paleo-Asian Ocean in Ordovician–early Silurian time was comparable in size with the modern Pacific Ocean.

Acknowledgements

The study was supported by the Ministry of Education and Science of the Russian Federation (project no. 14.Y26.31.0018), Scientific Project of the Institute of Geology and Mineralogy, Siberian Branch, Russian Academy of Sciences (state assignments no. 0330-2016-0003) and by a professorship program of the Centre for Northeast Asian Studies, the Tohoku University, Sendai, Japan from the Tohoku University (for IS).

Appendix A. Supplementary data

Supplementary data to this article can be found online at https://doi.org/10.1016/j.gr.2019.09.004.

References

Antonyuk, R.M., 1974. Oceanic crust of the eugeosynclinal region of east Central Kazakhstan. Tectonics of the Ural-Mongolian Fold Belt, Moscow ([in Russian]).
Avdeev, A.V., 1986. Geology of Ophiolitic Zones of Kazakhstan. Abstract of dissertation, Novosibirsk, p. 32 ([in Russian]).
Buslov, M.M., Saphonova, I.Yu, Watanabe, T., Obut, O., Fujiwara, Y., Iwata, K., Semakov, N.N., Sugai, Y., Smirnova, L.V., Kazansky, A.Yu, 2001. Evolution of the Paleo-Asian Ocean (Altai-Sayan region, Central Asia) and collision of possible Gondwana-derived terranes with the southern marginal part of the Siberian continent. Geosci. J. 5, 203–224.
Degtyarev, K.E., 2011. Tectonic evolution of early paleozoic island arc systems and continental crust formation in the caledonides of Kazakhstan and the north tien Shan. Geotectonics 45, 28–57.
Degtyarev, K.E., 2012. Tectonic Evolution of the Early Paleozoic Island Arc Systems and Formation of the Continental Crust in the Caledonides of Kazakhstan. GEOS, Moscow, p. 2012 ([in Russian]).
Dewey, J.F., Bird, J.M., 1970. Mountain belts and the new global tectonics. J. Geophys. Res. 75, 2625–2647.
Dobretsov, N.L., Berzin, N.A., Buslov, M.M., 1995. Opening and tectonic evolution of the Paleo-Asian Ocean. Int. Geol. Rev. 37, 335–360.
Dobretsov, N.L., Buslov, M.M., Vernikovsky, V.A., 2003. Neoproterozoic to early ordovician evolution of the Paleo-Asian Ocean: implications to the break-up of rodinia. Gondwana Res. 6, 143–159.
Ermolov, P.V., 2008. A new look at the origin of the ophiolite belts of Kazakhstan. Izvestia NAN RK, Seria geologic'eskaya 1, 76–85 ([in Russian]).
Ermolov, P.V., Stepanets, V.G., Sentov, N., 1990. Ophiolites of Kazakhstan. Guide of the excursion of the international workshop on the project №2 "Ophiolites. UT "Offset", Karaganda, p. 67 ([in Russian]).
Hadding, A.R., 1913. Undre dicellograptusskiffern i Skåne jämte några darmed ekvivalenta bildningar. Lunds Universitets Årsskrift N. F., Avd. 2, 1–90.
Hofmann, A.W., 1997. Mantle geochemistry: the message from oceanic volcanism. Nature 385, 219–229.
Hori, R., 1992. Radiolarian biostratigraphy at the triassic/jurassic period boundary in bedded cherts from the Inuyama area, Central Japan. J. Geosci. 35, 53–65.
Humphris, S.E., Thompston, G., 1978. Hydrothermal alteration of oceanic basalts by

seawater. Geochem. Cosmochim. Acta 42, 107–125.
Ichiyama, Y., Ishiwatari, A., Koizumi, K., 2008. Petrogenesis of greenstones from the Mino-Tamba belt, SW Japan: evidence for an accreted Permian oceanic plateau. Lithos 100, 127–146.
Isozaki, Y., Maruyama, S., Fukuoka, F., 1990. Accreted oceanic materials in Japan. Tectonophysics 181, 179–205.
Iwata, K., Sennikov, N.V., Buslov, M.M., Obut, O.T., Shokalsky, S.P., Kuznetsov, S.A., Ermikov, V.D., 1997. Upper Cambrian–Early Ordovician age of the Zasur'-iabasalt-chert-terrigenous formation (northwestern Gorny Altai). Russ. Geol. Geophys. 38, 1427–1444.
Jensen, 1976. A New Cation Plot for Classifying Subalkalic Volcanic Rocks – Ontario Division Mines Misc.
Jahn, B.-M., 2004. The central asian orogenic belt and growth of the continental crust in the phanerozoic. In: Malpas, J., Fletcher, C.J.N., Ali, J.R., Aitchison, J.C. (Eds.), Aspects of the Tectonic Evolution of China, vol. 226. Geological Society, London, Special Publication, pp. 73–100.
Koshkin, V.Y., Galitsky, V.V., 1960. Geological Map of the USSR. 1: 200 000. Series Balkhash. Sheet L-43-XI. South Kazakhstan Geological Department of the Ministry of Geology and Mineral Protection of the USSR ([in Russian]).
Koshkin, V.Y., Abdrakhmanov, B.M., Volkov, V.V., Mertenov, V.M., 1987. Stratigraphy of Ordovician and Silurian Terrigenous-Cherty-Basaltic Formation of North Balkhash Region. Regional Geology and Geophysics of Kazakhstan. KazIMS, Alma- Ata, pp. 6–15 ([in Russian]).
Kovalenko, I., Aerov, G., Bagrova, Z., 1994. Geological and structural conditions localizing ornamental stone occurrences in the ophiolites of the Itmurunda Zone, Kazakhstan. In: Ishiwatari, et al. (Eds.), Proceeding of the 29th International Geological Congress Part D, pp. 255–262.
Kröner, A., Windley, B., Badarch, G., Tomurtogoo, O., Hegner, E., Jahn, B.M., Gruschka, S., Khain, E.V., Demoux, A., Wingate, M.T.D., 2007. Accretionary growth and crust formation in the Central Asian orogenic belt and comparison with the Arabian-Nubian shield. In: Hatcher, R.D., Carlson, M.P., McBride, J.H., Martinez Catalan, J.R. (Eds.), Framework of Continental Crust. Geological Society of America Memoir 200, pp. 181–209.
Kröner, A., Kovach, V., Belousova, E., Hegner, E., Armstrong, R., Dolgopolova, A., Seltmann, R., Alexeiev, D.V., Hoffmann, J.E., Wong, J., Sun, M., Cai, K., Wang, T., Tong, Y., Wilde, S.A., Degtyarev, K.E., Rytsk, E., 2014. Reassessment of continental growth during the accretionary history of the central asian orogenic belt. Gondwana Res. 25, 103–125.
Kurenkov, S.A., Didenko, A.N., Simonov, V.A., 2002. Geodynamics of Paleospreading. GEOS, Moscow, p. 294 (in Russian).
Kurkovskaya, L.A., 1985. Complexes of conodonts from cherty and volcanogenic-cherty deposits of Ordovician of Central Kazakhstan. Geology of Early Syncline Complex of Central Kazakhstan. Izdatelstvo Moskovskogo Universiteta, pp. 164–177 ([in Russian]).
Le Maitre, R.W. (Ed.), Streckeisen, A., Zanettin, B., Le Bas, M.J., Bonin, B., Bateman, P., Bellieni, G., Dudek, A., Efremova, S., Keller, J., Sabine, P.A., Schmid, R., Sorensen, H., Woolley, A.R., 2002. Igneous Rocks: A Classification and Glossary of Terms, Recommendations of the International Union of Geological Sciences, Subcommission of the Systematics of Igneous Rocks. Cambridge University Press.
Kusky, T., Windley, B., Safonova, I., Wakita, K., Wakabayashi, J., Polat, A., Santosh, M., 2013. Recognition of Ocean Plate Stratigraphy in accretionary orogens through Earth history: a record of 3.8 billion years of sea floor spreading, subduction, and accretion. Gondwana Res. 24, 501–547.
Liu, B., Li, S., Suo, Y., Li, G., Dai, L., Somerville, I.D., Guo, L., Zhao, S., Yu, S., 2016. The geological nature and geodynamics of the okinawa trough, western pacific. Geol. J. 51, 416–428.
Maruyama, S., Liou, J.G., Terabayashi, M., 1996. Blueschists and eclogites of the world and their exhumation. Int. Geol. Rev. 38, 485–594.
Maruyama, S., Kawai, T., Windley, B.F., 2010. Ocean plate stratigraphy and its imbrication in an accretionary orogen: the Mona Complex, Anglesey-Lleyn, Wales, UK. In: Kusky, T.M., Zhai, M.-G., Xiao, W. (Eds.), The Evolving Continents: Understanding Processes of Continental Growth, vol. 338. Geological Society, London, Special Publications, pp. 55–75.
Maruyama, S., Omori, S., Sensu, H., Kawai, K., Windley, B.F., 2011. Pacific-type orogens: new concepts and variations in space and time from present to past. J. Geogr. 120, 115–223 (in Japanese with English abstract and captions).
Maruyama, S., Isozaki, Y., Kimura, G., Terabayashi, M., 1997. Paleogeographic maps of the Japanese Islands: plate tectonic synthesis from 750 Ma to the present. Isl. Arc 6, 121–142.
Matsuda, T., Uyeda, S., 1971. On the Pacific-type orogeny and its model - extension of the paired belts concept and possible origin of marginal seas. Tectonophysics 11, 5–27.
Matsuda, T., Isozaki, Y., 1991. Well-documented travel history of Mesozoic pelagic chert in Japan: remote ocean to subduction zone. Tectonics 10, 475–499.
Miyashiro, A., 1973. The Troodos ophiolitic complex was probably formed in an island arc. Earth Planet. Sci. Lett. 19, 218–224.
Mossakovsky, A.A., Ruzhentsev, S.V., Samygin, S.G., Kheraskova, T.N., 1993. The Central Asian fold belt: geodynamic evolution and formation history. Geotectonics 26, 455–473.
Neal, C.R., Mahoney, J.J., Kroenke, L.W., Duncan, R.A., Petterson, M.G., 1997. The ontong java plateau. In: Mahoney, J.J., Coffin, M.F. (Eds.), Large Igneous Provinces, Geophys, vol. 100. Monogr. Ser, pp. 183–216.
Nikitin, I.F., 2002. Ordovician siliceous and siliceous-basalt complexes of Kazakhstan. Russ. Geol. Geophys. 43, 512–527.
Nikitin, I.F., Frid, N.M., Zvontsov, V.S., 1991. Paleogeography and main features of volcanism in the ordovician of Kazakhstan and north tien Shan. In: Barnes, C.R., Williams, S.H. (Eds.), Advances in Ordovician Geology, vols. 90–9. Geological Survey of Canada, pp. 259–270.
Nikitin, I.F., Zhylkaidarov, A.M., Frid, N.M., 1992. Ordovician cherty-basaltic complex of the south-western Predchingiz region, izvestia NAN RK. Seria geologic'eskaya 4, 57–70 ([in Russian]).
Novikova, M.Z., Gerasimova, N.A., Dubinina, S.V., 1983. Conodonts from the volcanic-siliceous complex of the northern Balkhash. Doklady AN SSSR 271, 1449–1451 ([in Russian]).
Patalakha, F.A., Belyi, V.A., 1981. Ophiolites of the Itmurundy-Kazyk zone. In: Abdulin, A.A., Patalakha, F.A. (Eds.), Ophiolites of Kazakhstan. Nauka, Alma-Ata, pp. 7–102 ([in Russian]).
Polat, A., Kerrich, R., Wyman, D., 1999. Geochemical diversity in oceanic komatiites and basalts from the late Archean Wawa greenstone belts, Superior Province, Canada: trace element and Nd isotope evidence for a heterogeneous mantle. Precambrian Res. 94, 139–173.
Regelous, M., Hofmann, A.W., Abouchami, W., Galer, S.J.G., 2003. Geochemistry of lavas from the Emperor Seamounts, and the geochemical evolution of Hawaiian magmatism from 85 to 42 Ma. J. Petrol. 44, 113–140.
Romer, R.L., Heinrich, W., Schröder-Smeibidl, B., Meixner, A., Fischer, C.-O., Schulz, C., 2005. Elemental dispersion and stable isotope fractionation during reactive fluid flow and fluid immiscibility in the Bufa del Diente aureole, NE-Mexico: evidence from radiographies and Li, B, Sr, Nd, and Pb isotope systematics. Contrib. Mineral. Petrol. 149, 400–429.
Safonova, I.Yu, 2017. Juvenile versus recycled crust in the Central Asian Orogenic Belt: implications from ocean plate stratigraphy, blueschist belts and intra-oceanic arcs. Gondwana Res. 47, 6–27.
Safonova, I., Maruyama, S., 2014. Asia: a frontier for a future supercontinent Amasia. Int. Geol. Rev. 59, 1051–1071.
Safonova, I., Santosh, M., 2014. Accretionary complexes in the Asia-Pacific region: tracing archives of ocean plate stratigraphy and tracking mantle plumes. Gondwana Res. 25, 126–158.
Safonova, I.Y., Sennikov, N.V., Komiya, T., Bychkova, Y.V., Kurganskaya, E.V., 2011. Geochemical diversity in oceanic basalts hosted by the Zasur'ya accretionary complex, NW Russian Altai, Central Asia: implications from trace elements and Nd isotopes. J. Asian Earth Sci. 42, 191–207.
Safonova, I.Yu, Simonov, V.A., Kurganskaya, E.V., Obut, O.T., Romer, R.L., Seltmann, R., 2012. Late Paleozoic oceanic basalts hosted by the Char suture-shear zone, East Kazakhstan: geological position, geochemistry, petrogenesis and tectonic setting. J. Asian Earth Sci. 49, 20–39.
Safonova, I., Kojima, S., Nakae, S., Romer, R., Seltmann, R., Sano, H., Onoue, T., 2015. Oceanic island basalts in accretionary complexes of SW Japan: tectonic and petrogenetic implications. J. Asian Earth Sci. 113, 508–523.
Safonova, I., Maruyama, S., Kojima, S., Komiya, T., Krivonogov, S., Koshida, K., 2016. Recognizing OIB and MORB in accretionary complexes: a new approach based on ocean plate stratigraphy, petrology and geochemistry. Gondwana Res. 33, 92–114.
Safonova, I., Kotlyarov, A., Krivonogov, S., Xiao, W., 2017. Intra-oceanic arcs of the Paleo-Asian Ocean. Gondwana Res. 50, 167–194.
Safonova, I., Komiya, T., Romer, L.R., Simonov, V., Seltmann, R., Rudnev, S., Yamamoto, S., Sun, M., 2018. Supra-subduction igneous formations of the Char ophiolite belt, East Kazakhstan. Gondwana Res. 59, 159–179.
Safonova, I. Yu, Perfilova, A.A., Obut, O.T., Savinsky, I.A., Cherny, R.I., Petrenko, N.A., Gurova, A.V., Kotler, P.D., Khromykh, S.V., Krivonogov, S.K., Maruyama, S., 2019. Itmurundy accretionary complex (Northern Balkhash): geological structure, stratigraphy and tectonic origin. Russian Journal of Pacific Geology 38, 102–117.
Scotese, C.R., McKerrow, W.S., 1991. Ordovician plate tectonic reconstructions. In: Barnes, ChC., Williams, C.H. (Eds.), Advances in Ordovician Geology. Geological Survey of Canada, pp. 271–282. Paper 90-9.
Sengör, A.M.C., Natal'in, B.A., Burtman, V.S., 1993. Evolution of the altaid tectonic collage and paleozoic crustal growth in eurasia. Nature 364, 299–307.
Sennikov, N.V., Iwata, K., Ermikov, V.D., Obut, O.T., Khlebnikova, T.V., 2003. Oceanic sedimentation settings and fauna associations in the Paleozoic on the southern framing of the West Siberian Plate. Russ. Geol. Geophys. 44, 156–171.
Shen, B., Xiao, S., Dong, L., Zhou, C., Liu, J., 2007. Problematic macrofossils from Ediacaran successions in the North China and Chaidam blocks: implications for their evolutionary roots and biostratigraphic significance. J. Paleontol. 81, 1396—1411.
Stepanets, W.G., 2016. Ophiolites of Kazakhstan. Geology and Geodynamics. Acad. Publishing house Lambert, p. 251 [in Russian].
Sun, S., McDonough, W.F., 1989. Chemical and isotopic systematics of oceanic basalts: implications for mantle composition and processes. In: Saunders, A.D., Norry, M.J. (Eds.), Magmatism in the Ocean Basins, vol. 42. Geological Society, London, Special Publication, pp. 313–345.
Thompson, G., 1991. Metamorphic and hydrothermal processes: basalt–seawater interactions. In: Floyd, P.A. (Ed.), Oceanic Basalts. Blachie and Sons Ltd., Glasgow, pp. 148–173.
Valsami-Jones, E., Ragnarsdottir, K.V., 1997. Controls on uranium and thorium behaviour in ocean-floor hydrothermal systems: examples from the Pindos ophiolite, Greece. Chem. Geol. 135, 263–274.
Wakita, K., 2012. Mappable features of mélanges derived from Ocean Plate Stratigraphy in the Jurassic accretionary complexes of Mino and Chichibu terranes, Southwest Japan. Tectonophysics 568–569, 74–85.
Wang, Z., Sun, S., Li, J., Hou, Q., Qin, K., Xiao, W., Hao, J., 2003. Paleozoic tectonic evolution of the northern Xinjiang, China: geochemical and geochronological constraints from the ophiolites. Tectonics 22, 1–15.

Windley, B.F., Alexeiev, D., Xiao, W., Kroner, A., Badarch, G., 2007. Tectonic models for accretion of the central asian orogenic belt. Journal of the Geological Society of London 164, 31–47.
Yang, G.X., Li, Y.J., Santosh, M., Xiao, W.J., Yang, B.K., Tong, L.L., Zhang, S.L., 2015. Alkaline basalts in the Karamay ophiolitic mélange, NW China: a geological, geochemical and geochronological study and implications for geodynamic setting. J. Asian Earth Sci. 113, 110–125.
Yarmolyuk, V.V., Kuz'min, M.I., Vorontsov, A.A., 2013. West pacific-type convergent boundaries and their role in the formation of the central asian fold belt. Russ. Geol. Geophys. 54, 1427–1441.
Zhang, J., Xiao, W., Luo, J., Chen, Y., Windley, B.F., Song, D., Han, C., Safonova, I., 2018. Collision of the tacheng block with the mayile-barleik-tangbale accretionary complex in western junggar, NW China: implication for early-middle paleozoic architecture of the western altaids. J. Asian Earth Sci. 159, 259–278.
Zhylkaidarov, A.M., 1998. Conodonts form ordovician of Central Kazakhstan. Acta Paleontologica Polonica 43, 53–68.
Zonenshain, L.P., Kuzmin, M.I., Natapov, L.M., 1990. Geology of the USSR: A Plate Tectonic Synthesis. Geodynamic Monograph Series. American Geophysical Union, Washington.

Inna Safonova: Lab Chief at the Geology-Geophysics Department of the Novosibirsk State University; Senior Research Scientist at the Sobolev Institute of Geology and Mineralogy SB RAS, both in Novosibirsk, Russia. M.Sc. (1987) from the Novosibirsk State University (Honors), Ph.D. (2005) from the Institute of Geology SB RAS. Associate Editor of Gondwana Research (2017 Best Editor Award), Geoscience Frontiers (2016 Best Editor Award) and Journal of Asian Earth Sciences. Brain Pool Program Researcher in Korea Institute of Geology and Mineral Resources (2010–2012). Awardee of fellowship programs from JSPS at the Tokyo Institute of Technology (2014–2015) and University of Tokyo (2017), and CNEAS professorship program at Tohoku University (2019), all in Japan. Research fields include Pacific-type orogeny, ocean plate stratigraphy, geochronology, intra-plate and supra-subduction magmatism, mantle plumes. Leader of IGCP#592 Project "Continental construction in the Central Asian Orogenic Belt compared with actualistic examples from the western Pacific" under UNESCO-IUGS (2012–2016), Megagrant Project of the Ministry of Education and Science of Russia "A multidisciplinary study of Pacific-type orogenic belts and development of a holistic model linking evolution of oceans, their active margins and mantle magmatism" (grant no. №14.Y26.31.0018; 2017–2019) and co-leader of IGCP#592 Project "Orogenic architecture and crustal growth from accretion to collision: examples from the Central Asian Orogenic Belt and Tethyan orogen" (2017–2021).

Ilya Savinskiy: Research Scientist at the Institute of Geology and Mineralogy SB RAS (since 2009–2018) and at the Laboratory of Evolution of Paleo-Oceans and Mantle Magmatism (LEPOM) at the Geology-Geophysical Department of the Novosibirsk State University (since 2017), both in Novosibirsk, Russia. M.Sc. in Geology from the Novosibirsk State University (2012). Ph.D. in Petrology and Volcanology from the Institute of Geology and Mineralogy SB RAS (2017). Research fields includes structural geology and metamorphic petrology. Recent study regions: eastern Kazakhstan (Irtysh shear zone) and northern Balkhash (Itmurundy belt). Participant of Megagrant Project of the Ministry of Education and Science of Russia "A multidisciplinary study of Pacific-type orogenic belts and development of a holistic model linking evolution of oceans, their active margins and mantle magmatism" (grant no. №14.Y26.31.0018; 2017–2019).

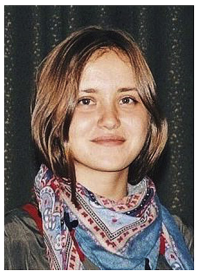

Alina Perfilova: Junior research scientist at the Laboratory of Evolution of Paleo-Oceans and Mantle Magmatism (LEPOM) at the Geology-Geophysical Department of the Novosibirsk State University; laboratory assistant at the Sobolev Institute of Geology and Mineralogy SB RAS, Novosibirsk, Russia. Got M.Sc. degree in Geology from the Novosibirsk State University in 2019 on "Geological position, age and composition of sandstones of the Itmurundy accretionary complex". Research fields include geology, geochemistry and geochronology of sedimentary rocks, ocean plate stratigraphy, Pacific-type orogenic belts. Participant of Megagrant Project no. №14.Y26.31.0018 from the Ministry of Education and Science of Russia "A multidisciplinary study of Pacific-type orogenic belts and development of a holistic model linking evolution of oceans, their active margins and mantle magmatism" (2017–2019).

Alexandra Gurova: Junior research scientist at the Laboratory of Evolution of Paleo-Oceans and Mantle Magmatism (LEPOM) at the Geology-Geophysical Department of the Novosibirsk State University. M.Sc. in Geochemistry from the Novosibirsk State University (2018) on "Mineralogy and petrography of gabbros from the Surovo-Talovka differentiated intrusion, eastern Kazakhstan". Scientific interests include igneous petrology, mineralogy and geochemistry, ocean plate stratigraphy, Pacific-type orogenic belts. Participant of Megagrant Project of the Ministry of Education and Science of Russia "A multidisciplinary study of Pacific-type orogenic belts and development of a holistic model linking evolution of oceans, their active margins and mantle magmatism" (no. №14.Y26.31.0018; 2017–2019).

Shigenori Maruyama is a professor at the Department of Earth and Planetary Sciences, Tokyo Institute of Technology, who graduated with a B.Sc. (1972) from Tokushima University, Japan, and received a Ph.D. (1981) from Nagoya Univ., Japan. He became an assistant professor at Toyama University in 1978, a post-doc at Stanford University, USA, moved to the University of Tokyo in 1991 as an associate professor, and in 1994 he became a professor at the Tokyo Institute of Technology. He undertook extensive fieldwork in Japan from 1971 to 1989, in California and the western coast of Canada from 1981 to 1989, and over the world since 1990, after he initiated the decoding of the Earth History program in over 25 countries. Since 1994 he has organized the multi-disciplinary program, 'Superplume Project' supported by STA, Japan, combining geophysics, isotope geochemistry, UHP experiments, and world geology. Major results from this work were published in the edited book, 'Superplumes; Beyond Plate Tectonics', Springer, Holland, 569 p. (2007). His current interest is the origin and evolution of life in the framework of Galaxy–Genome. At present he is a Leading Scientist of Megagrant Project of the Ministry of Education and Science of Russia "A multidisciplinary study of Pacific-type orogenic belts and development of a holistic model linking evolution of oceans, their active margins and mantle magmatism" (grant no. №14.Y26.31.0018; 2017–2019).